AFWL-TR-76-304

AFWL-TR-
76-304

UHF PROPAGATION EFFECTS IN SCINTILLATED ENVIRONMENTS

August 1977

Final Report

Approved for public release; distribution unlimited.

This research was sponsored by the Defense Nuclear Agency under Subtask S99QAXHB054, Work Unit 01, Work Unit Title, Propagation Models for Satellite Communications.

Prepared for
Director
DEFENSE NUCLEAR AGENCY
Washington, DC 20305

AIR FORCE WEAPONS LABORATORY
Air Force Systems Command
Kirtland Air Force Base, NM 87117

This final report was prepared by the Air Force Weapons Laboratory, Kirtland Air Force Base, New Mexico, under Job Order WDNB5401. Capt Wittwer (DYC) was the Laboratory Project Officer-in-Charge.

When US Government drawings, specifications, or other data are used for any purpose other than a definitely related Government procurement operation, the Government thereby incurs no responsibility nor any obligation whatsoever, and the fact that the Government may have formulated, furnished, or in any way supplied the said drawings, specifications, or toher data is not to be regarded by implication or otherwise as in any manner licensing the holder or any other person or corporation or conveying any rights or permission to manufacture, use, or sell any patented invention that may in any way be related thereto.

This report has been reviewed by the Information Office (OI) and is releasable to the National Technical Information Service (NTIS). At NTIS, it will be available to the general public, including foreign nations.

This technical report has been reviewed and is approved for publication.

Leon A. Wittwer
LEON A. WITTWER
Captain, USAF
Project Officer

FOR THE COMMANDER

John D. Hawkins
JOHN D. HAWKINS
Maj, USAF
Chief, Satellite and C^3 Branch

Paul J. Daily
PAUL J. DAILY
Colonel, USAF
Chief, Technology & Analysis Division

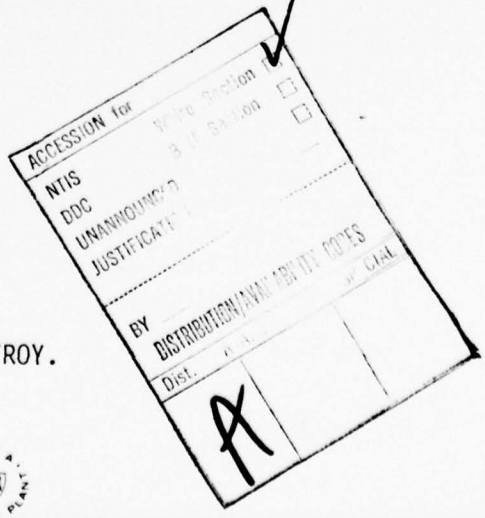

DO NOT RETURN THIS COPY. RETAIN OR DESTROY.

UNCLASSIFIED

SECURITY CLASSIFICATION OF THIS PAGE *(When Data Entered)*

REPORT DOCUMENTATION PAGE	READ INSTRUCTIONS BEFORE COMPLETING FORM
1. REPORT NUMBER (14) AFWL-TR-76-304	2. GOVT ACCESSION NO. / 3. RECIPIENT'S CATALOG NUMBER
4. TITLE *(and Subtitle)* (6) UHF PROPAGATION EFFECTS IN SCINTILLATED ENVIRONMENTS.	5. TYPE OF REPORT & PERIOD COVERED (9) Final Report,
	6. PERFORMING ORG. REPORT NUMBER
7. AUTHOR(s) (10) Leon A. Wittwer, Captain, USAF Ted Salvi, Captain, USAF Erle Pettus, Captain, USAF	8. CONTRACT OR GRANT NUMBER(s)
9. PERFORMING ORGANIZATION NAME AND ADDRESS Air Force Weapons Laboratory (DYM) Kirtland AFB, NM 87117	10. PROGRAM ELEMENT, PROJECT, TASK AREA & WORK UNIT NUMBERS 62704H WDNB5401
11. CONTROLLING OFFICE NAME AND ADDRESS Director Defense Nuclear Agency Washington, D.C. 20305 (12) 74p. (11)	12. REPORT DATE August 1977 13. NUMBER OF PAGES 74
14. MONITORING AGENCY NAME & ADDRESS *(if different from Controlling Office)* (16) WDNB, S99QAXH (17) 5H, B054	15. SECURITY CLASS. *(of this report)* UNCLASSIFIED 15a. DECLASSIFICATION/DOWNGRADING SCHEDULE

16. DISTRIBUTION STATEMENT *(of this Report)*

Approved for public release; distribution unlimited.

(18) SBIE (19) AD-E200 052

DDC DEC 12 1977 B

17. DISTRIBUTION STATEMENT *(of the abstract entered in Block 20, if different from Report)*

18. SUPPLEMENTARY NOTES

This research sponsored by the Defense Nuclear Agency under Subtask S99QAXHB054, Work Unit 01, Work Unit Title, Propagation Models for Satellite Communications.

19. KEY WORDS *(Continue on reverse side if necessary and identify by block number)*

Ionospheric Propagation
Radio Propagation
UHF Propagation
Striations
Scintillations

20. ABSTRACT *(Continue on reverse side if necessary and identify by block number)*

Calculational methods for examining the effects of striations on UHF signals are presented. The advantages of each method are discussed. Calculations are presented which illustrate the various expected effects on signals from different striation structures. The calculations demonstrate that for ambient environments Rayleigh signal statistics are a reasonable worst case representation. It is also shown that for most cases of interest the ionospheric fluctuation power spectral density or its equivalent is necessary and sufficient to calculate the required signal effects.

DD FORM 1 JAN 73 1473 EDITION OF 1 NOV 65 IS OBSOLETE

UNCLASSIFIED

SECURITY CLASSIFICATION OF THIS PAGE *(When Data Entered)*

213 150 /B

CONTENTS

ILLUSTRATIONS

ILLUSTRATIONS (CONTINUED)

SECTION I

INTRODUCTION

The purpose of this paper is to characterize scintillated UHF signal structures in expected propagation environments for either ambient or nuclear environments. The characterization of UHF scintillation effects is necessary for the evaluation of existing and proposed UHF satellite communications systems. UHF systems are likely to be very important for many years to come for several reasons. First, there already exists a great deal of UHF operational experience from which to draw in developing new systems. Second, UHF hardware technology is well developed, lowering system costs. Also, propagation through disturbed environments requires high rf power levels which favors lower frequencies with their higher dc to rf power conversion efficiency. Finally, UHF systems appear to be adequate for many important satellite communication applications despite their higher sensitivity to various propagation effects.

This paper consists of five sections. The next section defines the propagation environments used to examine the basic characteristics of UHF propagation. The third section discusses the propagation methods that are used. The fourth section presents the results of the propagation calculations and the implications regarding UHF systems. The final section will summarize the basic conclusions of this work.

SECTION II

PROPAGATION ENVIRONMENTS

The propagation environment is a layer containing electron density fluctuations lying perpendicular to the propagation line of sight (LOS). Figure 1 portrays the geometry and the relevant dimensions. The values for z_g and z_s were chosen to be a reasonable compromise between nuclear and ambient environments. The value of z_s may be realizable in nuclear environments and can be approached at low elevation angles in ambient environments.

The fluctuation statistics in the layer are isotropic in two dimensions, one of which is parallel to the LOS. No variation in electron density is assumed in the third dimension. The fluctuation statistics are uniform over the layer and are described, in part, by one of four correlation functions. The remainder of the statistical description is supplied by either assuming gaussian fluctuations or by using some explicit representation for the fluctuations. Both the gaussian assumption and explicit representations will be used to demonstrate that for sufficiently large z_s only the correlation functions or, equivalently, the second order-statistics are necessary for calculating propagation effects.

The electron density fluctuation correlation functions are characterized by the mean square electron density fluctuation, $\overline{\Delta n^2}$, an outer scale size, L, and possibly an inner scale size, ℓ. Except where otherwise noted the values of the outer and inner scale sizes will be 1.25 km and 30 meters respectively. The assumed value for L is the smallest measured length associated with high relative fluctuation power ($\overline{\Delta n^2}/\overline{n^2} = 0.8$) known to the authors. The value for the inner scale was chosen because measurements with about 30 meter resolution in scale size in the ambient ionosphere did not reveal an inner scale.

The first correlation function used to represent the electron density fluctuations is exponential in nature. A simple candidate form is

$$R_{K_\rho 2}(\varepsilon,\rho) \equiv \overline{n(z+\varepsilon,x+\rho)\, n(z,x)} \tag{1a}$$

$$R_{K_\rho 2}(\varepsilon,\rho) = \overline{\Delta n^2}\, e^{-(\varepsilon^2+\rho^2)^{1/2}/L} \tag{1b}$$

This case will be labeled as K_ρ^{-2} because the power spectral density corresponding to equation (1b) is proportional to K_ρ^{-2} for $K_\rho \geq 1/L$. Power spectral densities with this dependence are characteristic of ambient environments as seen in data from in situ measurements (refs. 1 through 4) and calculations (refs. 5 and 6). Equation (1) is usually used when the fluctuations are taken as gaussian distributed and $\ell << L$. When an explicit representation of $n(z,x)$ is required, the form in equation (1b) is slightly modified but retains the exponential nature.

To construct an explicit representation let us consider a group of randomly located gaussian rods of electron density in some area A where A is in a plane containing the LOS and other fluctuation coordinate. Let us further assume that there are on the averabe $\bar{N}/A$ rods distributed per unit area. The two-nsional electron density is then

$$n(z,x) = \sum_{i=1}^{N} n_o(a_i) e^{-[(x-x_i)^2 + (z-z_i)^2]/a_i^2} \tag{2}$$

where a_i and N are distributed according to

$$P_a(a_i) = \ell/\sqrt{2}a_i^2, \; a_i \geq \ell/\sqrt{2} \tag{3}$$

$$P_N(N) = \frac{\bar{N}^N e^{-\bar{N}}}{N!} \tag{4}$$

and

$$n_o(a_i) = \left\{ \overline{4\Delta n^2}\, A / \left[\bar{N}\ell L \pi^{3/2} \left(1 - \mathrm{erf}\left(\frac{\ell}{2L} \right) \right) \right] \right\}^{1/2} e^{-a_i^2/4L^2} \tag{5}$$

where $$\mathrm{erf}(x) = \frac{2}{\sqrt{\pi}} \int_0^x e^{-t^2}\, dt$$

Note that now both an inner and outer scale size is required.

After some manipulation, it can be shown that the one-dimensional correlation function and power spectral density are, respectively,

$$R_{K_\rho}\text{-}2(\varepsilon) = \frac{\overline{\Delta n^2}}{2}\left\{e^{\varepsilon/L}\left[1 - \operatorname{erf}\left(\frac{\ell}{2L} + \frac{\varepsilon}{\ell}\right)\right]\right.$$

$$\left. + e^{-\varepsilon/L}\left[1 - \operatorname{erf}\left(\frac{\ell}{2L} - \frac{\varepsilon}{\ell}\right)\right]\right\} \tag{6}$$

$$PSD(K_\rho) = \frac{\overline{2\Delta n^2 e}}{L}^{-\ell^2/4L^2}\left[\frac{e^{-K_\rho^2\ell^2/4}}{1/L^2 + K_\rho^2}\right] \tag{7}$$

The mean electron density is

$$\overline{n(z,x)} = \frac{\pi^{3/2}\overline{N}\, n_o(0)\ell L}{2^{1/2}}\left[1\text{-}\operatorname{erf}\left(\ell/2\sqrt{2}L\right)\right] \tag{8}$$

when $\ell << L$, equations (6) and (7) demonstrate the required statistical properties. It is also interesting to note that neither the power spectral density or the correlation function depend on $\overline{N}/A$. This means that $\overline{N}/A$ can be varied independent of the second order statistics. Intuitively, as $\overline{N}/A$ increases, the number of rods intersected by a straight line ray must increase or, conversely, the mean free path between intersections must decrease. Let us define a mean free path (MFP) as

$$MFP \equiv \left[\frac{\overline{N}}{A}\int_{\ell/\sqrt{2}}^{\infty} [2a][\sqrt{2}a/L][e^{-a^2/4L^2}]\, P_a(a)_{da}\right]^{-1} \tag{9}$$

This definition is analagous to conventional scattering theory where the integral represents the average scattering cross section weighted for the differing size and magnitude of the gaussian rods. A MFP will be used as the measure of thickness of scattering layers to determine when only the correlation function is sufficient to do the propagation. Evaluating the integral in equation (9), we have

$$MFP \equiv \left[\frac{2\bar{N}\ell\sqrt{\pi}}{A}\left(1 - \text{erf}\left(\frac{\ell}{2\sqrt{2}L}\right)\right)\right]^{-1} \tag{10}$$

The explicit representation just described may or may not resemble the actual environment for higher than second order statistics. The representation was developed only to study the dependence of the propagation on the higher order statistics by varying the MFP layer thickness or by comparing with the gaussion fluctuation assumption.

The second correlation function to be considered is the inverse of the K_ρ^{-2} case, that is, the correlation function is now power law. This will be referred to as the intermediate case.

$$R_{INT.}(\varepsilon,\rho) = \overline{\Delta n^2}/(1 + (\varepsilon^2+\rho^2)/2L^2)^{3/2} \tag{11}$$

The gaussian assumption on the fluctuations will always be used in this case. This case has been postulated for some types of disturbed environments.

The third correlation function used is a gaussian function.

$$R_g(\varepsilon,\rho) \approx \overline{\Delta n^2}\, e^{-(\varepsilon^2+\rho^2)/L^2} \tag{12}$$

This function is not necessarily thought to be characteristic of any type of environment but is used as a meaningful excursion from the K_ρ^{-2} case for comparison purposes. An explicit representation using gaussian rods can be found for this case. Again let us assume that there are $\bar{N}/A$ gaussian rods distributed on the average over the propagation region. The electron density is

$$n(z,x) = n_o \sum_{i=1}^{N} e^{-[(x-x_i)^2 + (z-z_i)^2]/a^2} \tag{13}$$

where the rod size and n_o are constant. Let

$$n_o = \left(\frac{\overline{4\Delta n^2 A}}{\bar{N} L^2 \pi} \right)^{1/2} \tag{14}$$

$$a = L/\sqrt{2} \tag{15}$$

N is distributed as in equation (4). The mean electron density is found from equations (13) and (14).

$$\overline{n(z,x)} = \left(\frac{\bar{N}}{A} \pi L^2 \overline{\Delta n^2} \right)^{1/2} \tag{16}$$

The two-dimensional correlation function of this representation is exactly equation (12). The two-dimensional power spectral density is found by transforming equation (12).

$$PSD_g(K_x, K_z) = \pi L^2 \overline{\Delta n^2}\ e^{-(K_x^2 + K_z^2)L^2/4} \tag{17}$$

Again, neither the correlation function in equation (12) nor the power spectral density in equation (17) is a function of $\bar{N}/A$. For this case one MFP is defined as $\left(\frac{\sqrt{2} L \bar{N}}{A} \right)^{-1}$. The correspondence between a MFP for this case and a MFP for the K_ρ^{-2} case is evident.

The last correlation function corresponds to a random distribution of uniform square striations with one side perpendicular to the LOS. The striations are L on an edge. This case was generated to examine the effects of sharp edges on the question of determining when third order or higher fluctuation statistics are important. The two-dimensional power spectral density and correlation function for this case are

$$PSD_{sq}(K_x, K_z) = \frac{16 \overline{\Delta n^2}}{L^2} \frac{\sin^2 \left(\frac{K_x L}{2} \right) \sin^2 \left(\frac{K_z L}{2} \right)}{K_x^2 K_z^2} \tag{18}$$

$$R_{sq}(\varepsilon, \rho) = \overline{\Delta n^2}\ (1 - |\rho|/L)(1 - |\varepsilon|/L) \tag{19}$$

where $|\rho| \leq L$ and $|\epsilon| \leq L$. The mean electron density is

$$\overline{n(z,x)} = \left(\frac{\overline{N}}{A}\,\overline{\Delta n^2}\,L^2\right)^{1/2} \tag{20}$$

A mean free path for this last case is $(\overline{N}L/A)^{-1}$.

SECTION III

PROPAGATION METHODS

Three different propagation methods will be discussed. The first two will be referred to as the Tatarskii multiscatter (TM) method and the multiple phase screen (MPS) method. These two methods are complementary in the sense that there are cases where only one or the other is practical and cases where both are applicable. The use of two methods in regions where both are applicable allows comparisons to check each method respectively to insure accurate computation. The third method called the Rytov approximation (RA) method is useful not so much in actual calculation as in the physical insight it gives particularly in the onset of amplitude and phase flucuations.

Tatarskii Multiscatter Propagation

The TM method has been previously described (ref. 7) and the following has, in part, been extracted from that discussion. Let the signal incident on the slab be

$$E(z,x) = \overline{(E(z)} + E_R(z,x) + i\, E_I(z,x))e^{iKz} \tag{21}$$

where $E(z)$ = mean field

$E_R(z,x)$ = in-phase quadrature component

$E_I(z,x)$ = out-of-phase quadrature component

z = coordinate along LOS

x = coordinate perpendicular to LOS

K = field wave number

The initial conditions on the field quantities are

$$\overline{E(0)} = 1.0 \tag{22a}$$

$$E_R(0,x) = E_I(0,x) = 0.0 \tag{22b}$$

Let us now define the complex autocorrelation function and the asymmetry autocorrelation functions, henceforth to be known as the G and F functions respectively.

$$G(z,\rho) = \overline{E(z)^2} + \overline{E_R(z,x)E_R(z,x+\rho)} + \overline{E_I(z,x)E_I(z,x+\rho)} \tag{23}$$

$$F(z,\rho) = \overline{E(z)^2} + \overline{E_R(z,x)E_R(z,x+\rho)} - \overline{E_I(z,x)E_I(z,x+\rho)} + 2i\,\overline{E_R(z,x)E_I(z,x+\rho)} \tag{24}$$

since $\overline{E_R(z,x)} = \overline{E_I(z,x)} = 0$ and $\overline{E_R(z,x)E_I(z,x+\rho)} = \overline{E_I(z,x)E_R(z,x+\rho)}$. Tatarskii (ref. 2) derived the equation of motion for G. The derivation for F follows in a similar manner involving the same assumptions. The equations of motion are

$$\frac{dF(z,\rho)}{dz} = \frac{i}{K}\frac{d^2F(z,\rho)}{d\rho^2} - K^2F(z,\rho)[A(z,0) + A(z,\rho)] \tag{25}$$

$$\frac{dG(z,\rho)}{dz} = -K^2G(z,\rho)[A(z,0) - A(z,\rho)] \tag{26}$$

where $$A(z,\rho) = \frac{1}{K^4}\left(\frac{2\pi e^2}{mc^2}\right)^2 \int_{-\infty}^{\infty} \overline{\Delta n(z,x)\Delta n(z',x+\rho)}\, dz' \tag{27}$$

$\Delta n = n - \bar{n}$

e = electron charge

m = electron mass

c = speed of light

The limitations on equations (25) and (26) are discussed in Tatarskii (ref. 8) and are summarized on the following page.

$$\lambda << \ell \tag{28a}$$

$$Z_s > \text{MFP} \tag{28b}$$

$$\lambda\alpha << 1 \tag{28c}$$

$$\sigma_\theta^2 << 1 \tag{28d}$$

$$\alpha z_s \sigma_\theta^2 << 1 \tag{28e}$$

$$L << X_m \tag{28f}$$

where λ = field wavelength

ℓ = inner fluctuation scale size

L = outer fluctuation scale size

α = mean field attenuation coefficient

σ_θ^2 = mean square scattering angle

X_m = backscattering attenuation distance

These limitations do not affect present work. Another implicit assumption is that $A(z,\rho)$ varies slowly with respect to z over the largest scale size of the fluctuations. The TM method is basically limited to two-dimensional problems except where the fluctuations are nearly isotropic around the propagation line of sight.

A propagation calculation using the TM method consists of the following. First the $A(z,\rho)$ function is generated. Next, equations (25) and (26) are solved in the particular geometry desired. The F and G functions along with the gaussian assumption on the quadrature components results in a complete statistical description of the propagated signal structure. These statistics are converted to time statistics by the transformation

$$\tau = \rho/\bar{v} \tag{29}$$

where $\bar{v}$ is an average velocity calculated by considering the various sources of time variation in the system. Finally sample signal structures are generated from the time dependent statistics using fourier techniques described in reference 9.

In addition to single frequency structures, the TM method can calculate frequency coherence bandwidths. The coherence function is defined as

$$H(z,\rho) = \overline{E^*_{K_1}(z,x)E_{K_2}(z,x+\rho)} \tag{30}$$

$$H(z,\rho) = \overline{E_{RK_1}(z,x)E_{RK_2}(z,x+\rho)} + \overline{E_{IK_1}(z,x)E_{IK_2}(z,x+\rho)}$$

$$+ i\left(\overline{E_{RK_1}(z,x)E_{IK_2}(z,x+\rho)} - \overline{E_{IK_1}(z,x)E_{RK_2}(z,x+\rho)}\right) \tag{31}$$

where K_1 = first frequency wave number

K_2 = second frequency wave number

and $H(z,\rho)$ contains the mean field component terms. The real part of $H(z,\rho)$ is defined as the frequency correlation coefficient. The imaginary part is the mean of the sine of the phase difference excluding dispersion between the two frequencies.

The equation of motion for $H(z,\rho)$ is

$$\frac{dH(z,\rho)}{dz} = i\frac{(K_1 - K_2)}{2K_1K_2}\frac{d^2H(z,\rho)}{d\rho^2} - \frac{K_p^4}{4K_1K_2}\left(\frac{(K_1^2 + K_2^2)}{2K_1K_2}A(z,0) - A(z,\rho)\right)H(z,\rho) \tag{32}$$

where $K_p^2 = 4\pi e^2/mc^2$. The form of the equation is similar to equation (25) and the same solution technique can be used. The initial condition is

$$H(0,\rho) = 1 \tag{33}$$

The coherence band width is defined as the value of $|K_1 - K_2|c/2 = |\nu_1 - \nu_2|$ where

$$\text{Real } [H(Z_g,0)] = 1/e = 0.368 \tag{34}$$

This coefficient is an estimate of the amount of band spreading required to get some measure of frequency diversity.

The TM method has both significant advantages and disadvantages. The basic advantages are simplicity, efficiency, and a large range of application. This method can handle much more severe conditions than the MPS or similar methods. The main disadvantage is that, for realistic propagation cases, it handles only either very weak scattering or Rayleigh multiscatter cases. These restrictions are a result of assuming gaussian statistics for the quadrature components. It is possible, in principle, to calculate the higher statistical moments using TM techniques and do away with the Rayleigh limitation, but, in practice, such calculations are too expensive to be practical. In addition, the gaussian assumption on the quadrature components is required for efficient generation of sample signals from the calculated statistics. These disadvantages are not very important as the MPS method handles these regions where the TM method is inadequate. In addition, it will later be apparent that the Rayleigh scatter case is the most common case for severe UHF environments.

Multiple Phase Screen Propagation

The field satisfies the following scalar wave equation.

$$(\nabla^2 + K^2 n_i^2(z,x))\, E(z,x) = 0 \tag{35}$$

where $n_i(z,x) = \overline{n_i} + \Delta n_i(z,x)$ = index of refraction

$$\overline{n_i} = \left(1 - \frac{4\pi e^2 \overline{n}}{mc^2 K^2}\right)^{1/2}$$

$\overline{n}$ = mean electron density

e = electron charge

m = electron charge

c = light speed

$K = 2\pi/\lambda$

λ = field wavelength

Making the usual parabolic approximation, we have

$$\left[\frac{\partial}{\partial z} - \frac{i}{2K\bar{n}_i}\frac{\partial^2}{\partial x^2} - iK\bar{n}_i\,\Delta n_i(z,x)\right] E'(z,x) = 0 \tag{36}$$

$$E'(z,x) = E(z,x)e^{-i\bar{n}_i Kz} \tag{37}$$

If $\Delta n_i(z,x) = 0$, the field propagation is exactly soluable.

$$E_f'(z+\Delta z,x) = \frac{1}{2T}\sum_{m=-\infty}^{\infty} C_m(z)e^{-\frac{1}{2K\bar{n}_i}\left(\frac{m\pi}{T}\right)^2 \Delta z}\, e^{i\frac{m\pi x}{T}} \tag{38}$$

where

$$C_m(z) = \int_{-T}^{T} E'(z,x)\, e^{-i\frac{m\pi x}{T}}\, dx \tag{39}$$

and $T \geq 5L$.

Equation (38) can be looked at as a sum of plane waves of wave number K indexed by m traveling at an angle of $\frac{m\pi}{TK\bar{n}_i}$ with respect to the z direction. The angles represented by $\frac{m\pi}{TK\bar{n}_i}$ are always very small for any m where $C_m(z)$ is significant. This means that the distance traveled by each plane wave is very close to Δz and hence each plane wave is affected in approximately the same way by $\Delta n_i(z,x)$. If $\Delta z \leq z_a$ where z_a is the distance a plane wave of wave number K can propagate without developing amplitude fluctuations, then the effects of the index of refraction fluctuations on each of the m waves is to shift the phase at $z+\Delta z$ by

$$\phi(x) = K\bar{n}_i \int_{z}^{z+\Delta z} \Delta n_i(z',x)dz' \tag{40}$$

The final propagated field at $z+\Delta z$ is approximately

$$E'(z+\Delta z,x) = E'_f\,(z+\Delta z,x)e^{i\phi(x)} \tag{41}$$

Equation (41) is the basis of the multiple phase screen propagation algorithm. The striated layer of thickness z_s is divided up into layers of thickness $\Delta z \leq z_a$. The propagation of the field through each successive layer is done according to equation (41). The determination of z_a will be discussed later in the discussion of the RA method. The MPS method is made practical primarily by the use of the fast fourier transform algorithm (FFT) to evaluate equations (38) and (39) because the FFT allows for a much more rapid transform than equation (39) suggests. The FFT produces a discrete, evenly spaced angular spectrum, which places another limitation on Δz. It is necessary that

$$m_{max}\left(\frac{\pi}{T}\right)^2 \frac{\Delta z}{K\bar{n}_i} \leq 1 \tag{42}$$

where $\left(\frac{m_{max}\pi}{T}\right)$ is the largest significant transverse field wave number.

The calculation of the integrated phase can be done in two ways. The first is explicit integration as shown in equation (40) which requires that $\Delta n_i(z,x)$ be specified. The second way is to determine $\phi(x)$ by Monte Carlo techniques assuming that Δn_i is a gaussian distributed variable. From equation (40)

$$\overline{\phi(x)\phi(x+\rho)} = \bar{n}_i^2K^2\int_z^{z+\Delta z} dz' \int_z^{z+\Delta z} dz''\ \overline{\Delta n_i(z',x)\Delta n_i(z'',x+\rho)} \tag{43}$$

Let $z'' = a' + \varepsilon$

$$\overline{\phi(x)\phi(x+\rho)} = \bar{n}_i^2K^2\int_z^{z+\Delta z} dz' \int_{z-z'}^{z+\Delta z-z'} d\varepsilon\ R_i(\varepsilon,\rho) \tag{44}$$

where $R_i(\varepsilon,\rho) = \overline{\Delta n_i(z,x)\,\Delta n_i(z+\varepsilon,x+\rho)}$ is the correlation function of the index of refraction fluctuations. If Δz is greater than several fluctuation correlation lengths, such that $R_i(\Delta z,\rho) = 0$, then

$$\overline{\phi(x)\phi(x+\rho)} = \Delta z\ \overline{n_i^2}\ K^2 \int_{-\infty}^{\infty} R_i(\varepsilon,\rho)\,d\varepsilon \tag{45}$$

Since $\Delta n_i(z,x)$ was assumed a gaussian distributed variable, $\phi(x)$ will be a gaussian distributed variable with the above correlation function. Let $\phi(x)$ be represented as a fourier series on the interval 2T.

$$\phi(x) = \frac{1}{2T} \sum_{m=-\infty}^{\infty} b_m\ e^{i\,\frac{m\pi x}{T}} \tag{46}$$

Since $\phi(x)$ is gaussian and zero mean, then so are the b_m. The variance of the b_m is easily shown to be

$$\overline{b_m^* b_j} = 2T \int_{-T}^{T} \overline{\phi(x)\phi(x+\rho)}\ e^{i\,\frac{m\pi x}{T}}\ \delta_{mj}\ d\rho \tag{47}$$

Also since $\phi(x)$ is real, $b_m = b_{-m}^*$. The generation of a realization is now rather easy. The fourier coefficients, b_m, are sampled from their known variance. Then FFT is used to evaluate equation (46) and $\phi(x)$ is then used in equation (41). The requirement that Δz be several fluctuation correlation lengths also means that successive calculations of $\phi(x)$ will be statistically independent.

The MPS method, like the TM method, has several advantages and limitations. The most important advantage is that the MPS method can handle the region in propagation space that includes weak scattering to near Rayleigh scattering which is the region that the TM method cannot handle. A second advantage is that when the FFT is used, the MPS is relatively fast and inexpensive so many cases can be run. The limitations on the MPS primarily stem from numerical

details. First, the method is practical only for two-dimensional problems due to computer considerations. This is not a very serious problem as propagation before the Rayleigh limit is reached is primarily two-dimensional. The most serious limitation on the MPS method derives from the practical limitation on the smallness of Δx, the transverse mesh spacing. As the propagation environment degrades the distance over which significant phase or amplitude changes occur becomes smaller. In practice, it is required that

$$\Delta x < \ell_o \approx \left[L/\left(\overline{K^2 \Delta n_i^2}\, z_s\right)\right]^{1/2} \tag{48}$$

This restriction limits the severity of effects that can be handled by the MPS method. Fortunately, calculations show that UHF signals become Rayleigh before Δx becomes so small as to make MPS calculations impractical. The TM method can be used in the Rayleigh regime after the MPS fails.

Rytov Approximation Method

The field must satisfy the scalar wave equation in equation (35).

Let

$$\psi(z,x) = \log\left(E(z,x)\right) \tag{49}$$

Then

$$\nabla^2\psi + (\nabla\psi)^2 + K^2 n_i^2(z,x) = 0 \tag{50}$$

Let

$$\psi(z,x) = \psi_o(z,x) + \psi_1(z,x) \tag{51}$$

and

$$n_i(z,x) = \bar{n}_i + \Delta n_i(z,x) \tag{52}$$

where

$\psi_o(z,x)$ and $\bar{n}_i$ satisfy equation (50) for the unperturbed case,

$$\nabla^2\psi_o + (\nabla\psi_o)^2 + \bar{n}_i^2 K^2 = 0 \tag{53}$$

If

$$|\Delta n_i(z,x)| << 1 \tag{54}$$

$$|\nabla\psi_1| << |\nabla\psi_o| \tag{55}$$

Then

$$\nabla^2\psi_1 + 2\nabla\psi_o \cdot \nabla\psi_1 + 2\bar{n}_i K^2 \Delta n_i(z,x) = 0 \tag{56}$$

If $\psi_1 = \chi + i\phi$, then after much manipulation (ref. 8) it can be shown

$$\overline{\chi(x)\chi(x+\rho)} = K^2 \int_{-\infty}^{\infty} \frac{dK_\rho}{2\pi} \int_0^{z_s} dz \sin^2\left[\frac{K_\rho^2}{2K}(z_s+z_g-z)\right] \int_{-\infty}^{\infty} d\varepsilon \tilde{C}_i(z,\varepsilon,K_\rho) e^{+iK_\rho\rho} \tag{57}$$

$$\overline{\phi(x)\phi(x+\rho)} = K^2 \int_{-\infty}^{\infty} \frac{dK_\rho}{2\pi} \int_0^{z_s} dz \cos^2\left[\frac{K_\rho^2}{2K}(z_s+z_g-z)\right] \int_{-\infty}^{\infty} d\varepsilon \tilde{C}_i(z,\varepsilon,K) e^{+iK_\rho\rho} \tag{58}$$

where

$$\tilde{C}_i(z,\varepsilon,K) = \int_{-\infty}^{\infty} \overline{\Delta n_i(z,x)\Delta n_i(z+\varepsilon,x+\rho)}\, e^{-iK_\rho\rho}\, d\rho \tag{59}$$

The z dependence in $C_i(z,\varepsilon,K_\rho)$ represents changes in the index of refraction statistics along the propagation line of sight. This method has all the basic restrictions of the TM method. In addition, it is required that $\overline{\chi^2} \lesssim 0.3$. The basic value of this method is that it gives insight into the onset and development of amplitude fluctuations, and phase fluctuations due to propagation.

Examination of equations (57) and (58) provides a prescription for determining when amplitude fluctuations occur and their dependence on the environment properties. First if

$$\frac{L^2K}{z_s+z_g} << 1 \tag{60a}$$

$$\tilde{C}_i(z,\varepsilon,K_\rho) = \tilde{C}_i(0,\varepsilon,K_\rho) \tag{60b}$$

then

$$\overline{\chi^2} \approx \left(\frac{2\pi e^2}{mc^2}\right)^2 \frac{z_s L}{K^2}\,\overline{\Delta n^2} \tag{61}$$

$$\overline{\phi^2} \approx \left(\frac{2\pi e^2}{mc^2}\right)^2 \frac{z_s L}{K^2}\,\overline{\Delta n^2} \tag{62}$$

For this case, the amplitude and phase fluctuations occur simultaneously. This is typical of VHF satellite links. If condition (60a) is not true then the results depend on the particular power spectrum assumed. When $\frac{L^2K}{z_s+2g} >> 1$,

$$\overline{\chi^2} \approx \frac{1}{12}\,\frac{[(z_s+z_g)^3-z_g^3]}{K^4}\,\overline{\Delta n^2}\left(\frac{2\pi e^2}{mc^2}\right)^2 \int_{-\infty}^{\infty} d\varepsilon \int_{-\infty}^{\infty} \frac{dK_\rho}{2\pi} K_\rho^4\, \tilde{C}(\varepsilon,K_\rho) \tag{63}$$

For a gaussian spectrum, equation (63) is exactly calculable.

$$\overline{\chi_g^2} \approx \sqrt{\pi}\,\frac{[(z_s+z_g)^3 - z_g{}^3]\overline{\Delta n^2}}{K^4L^3}\left(\frac{2\pi e^2}{mc^2}\right)^2 \tag{64}$$

For the K_ρ^{-2} spectrum, things get more complicated since

$$\int_{-\infty}^{\infty} \tilde{C}(\varepsilon,K_\rho)d\varepsilon \approx \frac{2\pi/L}{(1/L^2 + K_\rho^2)^{3/2}} \tag{65}$$

until the inner scale is reached. This means that the integrand in equation (63) increases until the spectrum inner scale is reached or until $\frac{K^2_\rho (z_s+z_g)}{K} = \pi$.

After some manipulation

$$\overline{\chi^2} \approx C_1\overline{\Delta n^2}\left(\frac{2\pi e^2}{mc^2}\right)^2 \frac{\left\{\left[(z_s+z_g)^3 - z_g^3\right]z_s\right\}^{1/2}}{K^3L}, \quad \frac{L^2K}{z_s+z_g} > 1 \tag{66}$$

where C_1 is a constant that was found by direct calculation to be approximately equal to 0.5.

Let us summarize. For the K_ρ^{-2} spectrum we have

$$\overline{\chi^2} \approx \left(\frac{2\pi e^2}{mc^2}\right)^2 \overline{\Delta n^2}\,\frac{z_s L}{K^2}, \quad \frac{L^2K}{z_s+z_g} < 1 \tag{67a}$$

$$\overline{\chi^2} \approx \left(\frac{2\pi e^2}{mc^2}\right)^2 0.5\,\overline{\Delta n^2}\,\frac{\left\{\left[(z_s+z_g)^3 - z_g^3\right]z_s\right\}^{1/2}}{LK^3}, \quad \frac{L^2K}{z_s+z_g} > 1 \tag{67b}$$

For the gaussian spectrum we have

$$\overline{\chi^2} \approx \left(\frac{2\pi e^2}{mc^2}\right)^2 \overline{\Delta n^2}\, \frac{z_s L}{K^2}, \quad \frac{L^2 K}{z_s+z_g} < 1 \tag{68a}$$

$$\overline{\chi^2} \approx \overline{\Delta n^2} \left(\frac{2\pi e^2}{mc^2}\right)^2 \sqrt{\pi}\, \frac{[(z_s+z_g)^3 - z_g^3]}{K^4 L^3}, \quad \frac{L^2 K}{z_s+z_g} > 1 \tag{68b}$$

The initial phase fluctuations go as

$$\overline{\phi^2} = \left(\frac{2\pi e^2}{mc^2}\right)^2 \frac{z_s}{K^2} L\, \overline{\Delta n^2}, \quad \frac{L^2 K}{z_s+z_g} < 1 \tag{69a}$$

$$\overline{\phi^2} = 2\left(\frac{2\pi e^2}{mc^2}\right)^2 \frac{z_s}{K^2} L\, \overline{\Delta n^2}, \quad \frac{L^2 K}{z_s+z_g} > 1 \tag{69b}$$

for either spectrum.

In general, equations (67b), (68b), and (69b) are usually appropriate. By taking the ratio of equation (68b) to equation (67b) we get

$$\frac{\overline{\chi_g^2}}{\overline{\chi_{K_\rho^{-2}}^2}} \approx \frac{2\sqrt{\pi}}{KL^2} \left[\frac{(z_s+z_g)^3 - z_g^3}{z_s}\right]^{1/2} \tag{70}$$

For $\frac{KL^2}{z_g+z_s} >> 1$, the K_ρ^{-2} spectrum results in a quicker onset of amplitude fluctuations. Taking the ratio of equations (67b) and (69b) we get

$$\frac{\overline{\chi^2}}{\overline{\phi^2}} \approx \frac{0.25}{KL^2} \left[\frac{(z_s+z_g)^3 - z_g^3}{z_s}\right]^{1/2} \tag{71}$$

which means that the phase fluctuations onset before the amplitude fluctuations. This is observed in ambient environments and in the calculations to follow. These equations show the advantages of maximizing K.

SECTION IV

RESULTS

The calculations to be discussed all assumed a nominal UHF frequency of 300 Mhz. The initial field strength and field amplitude was unity.

Figures 2 through 7 show several quadrature component correlation functions for the K_ρ^{-2} and intermediate spectrums. Several of these figures compare the TM and MPS results for identical scenarios and show good agreement. The agreement for the strong scatter cases is within the statistical noise of the MPS calculation. When the signal structure is Rayleigh, these correlation functions completely define the signal statistics and sample signals can be generated using methods discussed in reference 7. Even when the statistics are not Rayleigh, these correlation functions are very useful because their width is a measure of the signal structure correlation distance when the mean square phase is greater than about one. Let us define the correlation distance (ℓ_o) as the e^{-1} point of the correlation function curve. Figure 8 shows ℓ_o as a function of the environment parameters for the K_ρ^{-2} and the intermediate spectrums. In figure 8 a distinction is made between an outer scale size parallel to the propagation line of sight ($L_{\parallel}$) and a perpendicular outer scale size ($L_{\perp} = 1.25 \times 10^5$). This separation is necessary to parameterize the behavior of ℓ_o. For layers with uniform statistical properties ℓ_o can be adequately represented by a power law function.

$$\ell_o \propto L_{\perp}(L_{\parallel}\ \overline{\Delta n^2}\ z_g/K^2)^{-n} \tag{72}$$

For nonuniform layers the ℓ_o can be expressed as a power law function of an appropriately defined integral. Let us define for the K_ρ^{-2} and the intermediate spectrum an integral called the scale size factor.

$$SSF_{K_\rho^{-2}} = \int_0^{Z_s} \frac{L_{\parallel}\ \Delta n^2\ dz}{K^2 L_{\perp}^{1.623}} \tag{73}$$

$$SSF_{Int.} = \int_0^{Z_s} \frac{L_{\shortparallel} \overline{\Delta n^2}\, dz}{K^2 L_{\perp}^{1.941}} \tag{74}$$

Then

$$\ell_o = 2.4 \times 10^{14}\, SSF_{K_\rho^{-2}}^{-0.616} \tag{75}$$

$$\ell_o = 1.24 \times 10^{12}\, SSF_{Int.}^{-0.515} \tag{76}$$

The fit for the K_ρ^{-2} spectrum assumes that the environment inner scale size is zero. The curve set by the X-s assumed a 10 meter inner scale and hence the curve breaks upward as ℓ_o = 10 meters is approached. The slope of the "X" curve approaches minus one half asymptotically as the scale size factor increases.

If <v> is the velocity of the line of sight across the striations, then the correlation time τ_o can be defined.

$$\tau_o = \ell_o / \langle v \rangle \tag{77}$$

Thus equations (73) through (76) with <v> define for the two discussed spectra the basic time dependence of the signal parameters for mean square angles greater than one. Examination of figures 4 through 7 also shows that the correlation functions are approximately gaussian in shape so only one parameter is necessary to define the second order signal statistics. Thus for Rayleigh statistics, the statistical description is complete with one parameter. This is an important result in that it implies that in Rayleigh environments system performance is only a function of τ_o and the signal-to-noise ratio.

For the case where the signal disturbances are mainly phase fluctuation with little or no amplitude fluctuation, ℓ_o can be related to the phase correlation function. Let

$$\overline{\phi(x)\phi(x+\rho)} = \overline{\phi^2}\, F(\rho) \tag{78}$$

If $\phi(x)$ is gaussian distributed, as postulated for thick layers, then it can be shown from equation (26) that

$$\overline{E^*(x)E(x+\rho)} = E_0^2\, e^{-\overline{\phi^2}\,(1-F(\rho))} \tag{79}$$

Then

$$F(\ell_0) \simeq 1 - \frac{1}{\overline{\phi^2}} \tag{80}$$

when $\overline{\phi^2} >> 1$. Equation (78), which defines $F(\rho)$, and equation (80) demonstrate a clear link between ℓ_0 and the phase fluctuations. If we assume

$$F(\rho) \simeq 1 - \rho^2/\rho_0^2 + \text{---} \tag{81}$$

$$\overline{E^*(x)E(x+\rho)} \simeq 1 - \rho^2/\ell_0^2 + \text{--} \tag{82}$$

then

$$\rho_0^2 = \overline{\phi^2}\ell_0^2 \simeq L^2 \tag{83}$$

Equation (83) demonstrates the basic relationship between ρ_0, the phase correlation distance, and ℓ_0. Equation (83) also shows that the phase correlation distance is proportional to the root-mean-square phase fluctuation, a fact ignored in many works. Let us estimate the rate of change of the phase since this is the important quantity.

$$\frac{d\phi}{dx} \simeq \frac{\overline{\phi^2}^{1/2}}{\overline{\phi^2}^{1/2}\ell_0} \simeq \frac{1}{\ell_0} \tag{84}$$

This shows that the mean square phase fluctuation which is often used to estimate possible system degradation in reality contains little useful information without accompanying knowledge of L or ℓ_o.

Figures 9 through 13 show the quadrature component distribution functions for the K_ρ^{-2} spectrum as $\overline{\Delta n^2}$ increases. The solid curves in the last two component distribution functions are gaussian curves which show the distribution limit as $\overline{\Delta n^2}$ becomes large. These plots show that the amplitude fluctuations become significant with only a few radians of root-mean-square phase fluctuation. Indeed, as the component correlation functions become equal the amplitude fluctuations result in a near unity scintillation index. The statistics become essentially gaussian when $\overline{\Delta n^2} \simeq 10^{10}$.

Figures 14 through 17 and 18 through 23 show the component distributions for the intermediate and gaussian spectrum respectively. The results for the intermediate spectrum is little different from the gaussian so only the latter will be discussed. As with the K_ρ^{-2} spectrum, the component distributions become equal after a few radians of root-mean-square fluctuation. The amplitude fluctuations, however, develop more slowly with a different character. The population of deep fades is less than with the K_ρ^{-2} spectrum up to $\overline{\Delta n^2} = 10^{+10}$ and then exceeds the K_ρ^{-2} spectrum before settling down to a Rayleigh distribution at $\overline{\Delta n^2} = 10^{12}$. The population of a signal enhancements follows no simple behavior. The sides of the component distributions for the gaussian spectrum are steep, dipping below the gaussian distribution but going above for very large amplitudes. This behavior is simple to understand. For the gaussian spectrum there is essentially a single size of fluctuations at about $K_\rho^{-1} = 1.25$ km. The receiver at $z_g = 200$ km is in the near zone until $\overline{\Delta n^2}$ becomes very large. The initial propagation effects manifest themselves as large phase fluctuations with only small amplitude fluctuations. Eventually, amplitude fluctuations develop as $\overline{\Delta n^2}$ increases. The K_ρ^{-2} spectrum has the same large size as the gaussian but also has a significant population of smaller sizes whose zone the receiver is in or near. This gives rise to amplitude fluctuations at much smaller fluctuation power than does the gaussian spectra.

Additional insight is gained by examining figures 24 through 27 which are selected amplitude distributions for the three spectrums. These plots illustrate the observations made from the component distributions. The population of fades of a given depth is particularly apparent. Initially, the K_ρ^{-2} spectrum

gives the largest population of deep fades but the gaussian spectrum soon catches up. An important point in the K_ρ^{-2} amplitudes is that the population of deep fades is never greater than the Rayleigh limit. This means that for systems that are primarily sensitive to fades, the Rayleigh limit is the worst case for a K_ρ^{-2} spectrum. For the gaussian spectrum the situation is quite different. Let us assume that the fades are slow and that a system has 10 dB link margin. The performance will be a function of the population of fades with amplitudes less than 0.316. It's clear from figure 27 that for $\overline{\Delta n^2} \geq 3.2 \times 10^{10}$, the gaussian spectrum will result in a poorer performance than the Rayleigh limit.

The difference between the K_ρ^{-2} and the gaussian spectrums can be seen in figure 28 which contains the six-bit character error rate curve for the Tactical Transmission System (TATS) wideband modem. This system is a 8-array Frequency shift key UHF modem that was studied in detail in a previous work (ref. 9). The same model was used here. The solid curve is from the K_ρ^{-2} spectrum. For this spectrum the statistics are Rayleigh for $\tau_o \leq 0.5$ seconds. The remainder of the curve reflects the system performance as the Rayleigh limit is approached and is, in general, a function of more than τ_o. The important point to note is that in the approach to Rayleigh statistics, the performance was always better than that associated with the Rayleigh limit confirming the earlier discussion about the K_ρ^{-2} amplitude distribution. For the gaussian case, the Rayleigh limit is not reached until $\tau_o \leq 3 \times 10^{-2}$ seconds at which point the two curves are nearly convergent. Sine the K_ρ^{-2} curve represents the Rayleigh limit, it's clear that the gaussian spectrum gives performance which is worse than Rayleigh as was suggested earlier.

The basic issue for power spectra in UHF propagation is whether real spectrums are most often multisize such as the K_ρ^{-2} or single size like the gaussian. If K_ρ^{-2} is the rule, then Rayleigh statistics with given τ_o pose a reasonable worst case threat to UHF systems. At least ninety percent of ambient scintillation measurements have been K_ρ^{-2}, so reasonable worst case analysis is possible. For other disturbed environments, the correct spectrum or spectrums are not yet well defined. This study suggests that emphasis should be put on resolving the power spectrum unknowns.

The last question to be examined is the affect of third order or higher striation statistics on the propagation results. Figure 29 contains the amplitude distributions, S_4^2, and ℓ_o as a function of the mean-free-path thickness of the scattering layer for a gaussian power spectral density. The infinite mean-free-path case represents gaussian distributed fluctuations. Despite the statistical jitter in the caluclations the thinest case is clearly different from the thickest case. It appears that five to ten mean free paths are needed to get reasonable insensitivity to environment statistics above second order.

Figures 30 and 31 show the same propagation information as figure 29, only the power spectral density is now K_ρ^{-2} with the parameters as shown in the figures. These figures imply that three or more mean free paths are sufficient to become insensitive to the higher order.

Figures 32 and 33 repeat figures 30 and 31 with the inner scale essentially zero and including gaussian distributed fluctuations. Figure 34 repeats the calculations represented in figure 33 with $\overline{\Delta n^2}$ reduced to 3.33×10^8 and with the phase plotted instead of the amplitude. Again, as above, only a few mean free paths are necessary to randomize the phase and become dependent only on the first and second order fluctuation statistics.

Figure 35 contains results assuming square top hat striations. The sharp edges scatter so effectively that three mean free paths agree closely with assuming gaussian fluctuations.

It appears clear that, for most applicatons, the second order statistics or, equivalently, the fluctuation correlation function is a necessary and sufficient environment description for propagation purposes. The higher order statistics can be supplied by any reasonable assumption such as gaussian distributed fluctuations.

SECTION V

CONCLUSIONS

This paper has examined the propagation of electromagnetic signals through a region with fluctuations in the index of refraction. The region was assumed to be a thick multiscatter layer characterized by one of four types of power spectral densities. These power spectrums were called the K_ρ^{-2}, intermediate, gaussian, and square top hat power spectrums. The calculation results indicated that the intermediate and the gaussian cases were sufficiently similar that only one of them, the gaussian, was discussed in detail.

The K_ρ^{-2} spectrum is by far the most common measured spectrum in disturbed natural environments. The outer scale size associated with the largest measured fluctuation power, $\overline{\Delta n^2}/\overline{n^2} = 0.8$, is L = 1.25 km. This spectrum is considered by some to be a candidate for nuclear disturbed environments. The gaussian, intermediate, and square striation spectrum have also been used for disturbed environment. These spectrums vary from the K_ρ^{-2} spectrum in that they are characterized by a single size. Examination of turbulence spectrums reveals that the K_ρ^{-2} and the gaussian spectrum bracket the reasonable range of spectrums. The basic conclusions concerning propagation through these spectrums are:

1. The onset of phase and amplitude fluctuations is determined by setting $\overline{\chi^2} = \overline{\phi^2} = 0.1$ in the following equations and assuming constant statistical properties.

   If $\frac{L^2K}{z_s+z_g} < 1$, then

$$\overline{\chi^2} \approx \left(\frac{2\pi e^2}{mc^2}\right)^2 \overline{\Delta n^2}\, \frac{z_s L}{K^2} \qquad (67a)$$

$$\overline{\phi^2} = \overline{\chi^2}$$

   If $\frac{L^2K}{z_s+z_g} > 1$, then

$$\overline{\chi^2} = \left(\frac{2\pi e^2}{mc^2}\right)^2 \overline{\Delta n^2}\ 0.5\ \frac{\left\{\left[(z_s+z_g)^3 - z_g^3\right] z_s\right\}^{1/2}}{LK^3} \quad (K_\rho^{-2} \text{ spectrum}) \tag{67b}$$

$$\overline{\chi^2} = \left(\frac{2\pi e^2}{mc^2}\right)^2 \overline{\Delta n^2}\ \sqrt{\pi}\ \frac{\left[(z_s+z_g)^3 - z_g^3\right]}{K^4 L^3} \quad \text{(gaussian spectrum)} \tag{68b}$$

$$\overline{\phi^2} = \left(\frac{2\pi e^2}{mc^2}\right)^2 \Delta n^2\ 2\ \frac{z_s L}{K^2} \tag{69b}$$

2. The Rayleigh limit is a reasonable worst case for the K_ρ^{-2} spectrum for UHF signals. This means that the reasonable worst case performance of UHF systems can be parameterized with only two parameters, τ_o and the signal to noise ratio. The Rayleigh limit is not a worst case for the gaussian specturm. For this latter case, there is a focusing region where the population of deep fades exceed the Rayleigh case. This case does not appear to be significant because of a low probability of occurrence.

3. The distance (ℓ_o) over which the phase or amplitude can change significantly is specified by the following equations. For the K_ρ^{-2} spectrum, we get

$$SSF = \int_o^{z_s} \frac{L_{11} \Delta n^2\ dz}{K^2 L_1^{1.623}} \tag{73}$$

$$\ell_o = 2.4 \times 10^{14}\ SSF^{-0.616} \tag{75}$$

For the intermediate spectrum, we get

$$SSF = \int_o^{z_s} \frac{L_{11} \Delta n^2\ dz}{K^2 L_1^{1.941}} \tag{74}$$

$$\ell_o = 1.24 \times 10^{12}\ SSF^{-0.515} \tag{76}$$

4. For both spectrums, 5 to 10 mean free paths are sufficient to become sensitive only to the fluctuation correlation function. This conclusion is very important as it implies that for most cases of interest, only a limited amount of environment information is required.

REFERENCES

1. Kelley and Mozer, Cornell University, private communication.

2. Phelps, A. D. R., and Sagalyn, R. C., "Plasma Density Irregularities in the High-Latitude Top Side Ionosphere," Journal of Geophysical Research, Vol. 81, No. 4, 1 February 1976.

3. Dyson, P. L., McClure, J. P., and Hanson, W. B., "In Situ Measurements of the Spectral Characteristics of F Region Ionospheric Irregularities," Journal of Geophysical Research, Vol. 79, 1 April 1974.

4. Morse, F. A., et al., "EQUION, An Equatorial Ionospheric Irregularity Experiment," Aerospace Corporation, El Segundo, California, SSL-76(6960-04)-2, April 1976.

5. Scannapieco, A. J., Ossakow, S. L., Goldman, S. R., and Pierre, J. M., "Late-Time Striation Spectra," Naval Research Laboratory, private communication, February 1976.

6. Ragnlien, T. O., and Weinstock, J., "Theory of the Nonlinear Spectrum of the Gradient Drift Instability in the Equatorial Electrojet," Journal of Geophysical Research, Vol. 79., No. 31, 1 November 1974.

7. Wittwer, L. A., "Satellite Communications in a Scintillated Environment," AFWL-TR-75-240, Air Force Weapons Laboratory, Kirtland Air Force Base, New Mexico, January 1976.

8. Tatarskii, V. I., "The Effects of the Turbulent Atmosphere on Wave Propagation," National Science Foundation, TT-68-50464, 1971.

9. Wittwer, L. A., and Pettus, E., "The Performance of the TATS Modem in Scintillated Environments," AFWL-TR-76-128, Air Force Weapons Laboratory, Kirtland Air Force Base, New Mexico, 1976.

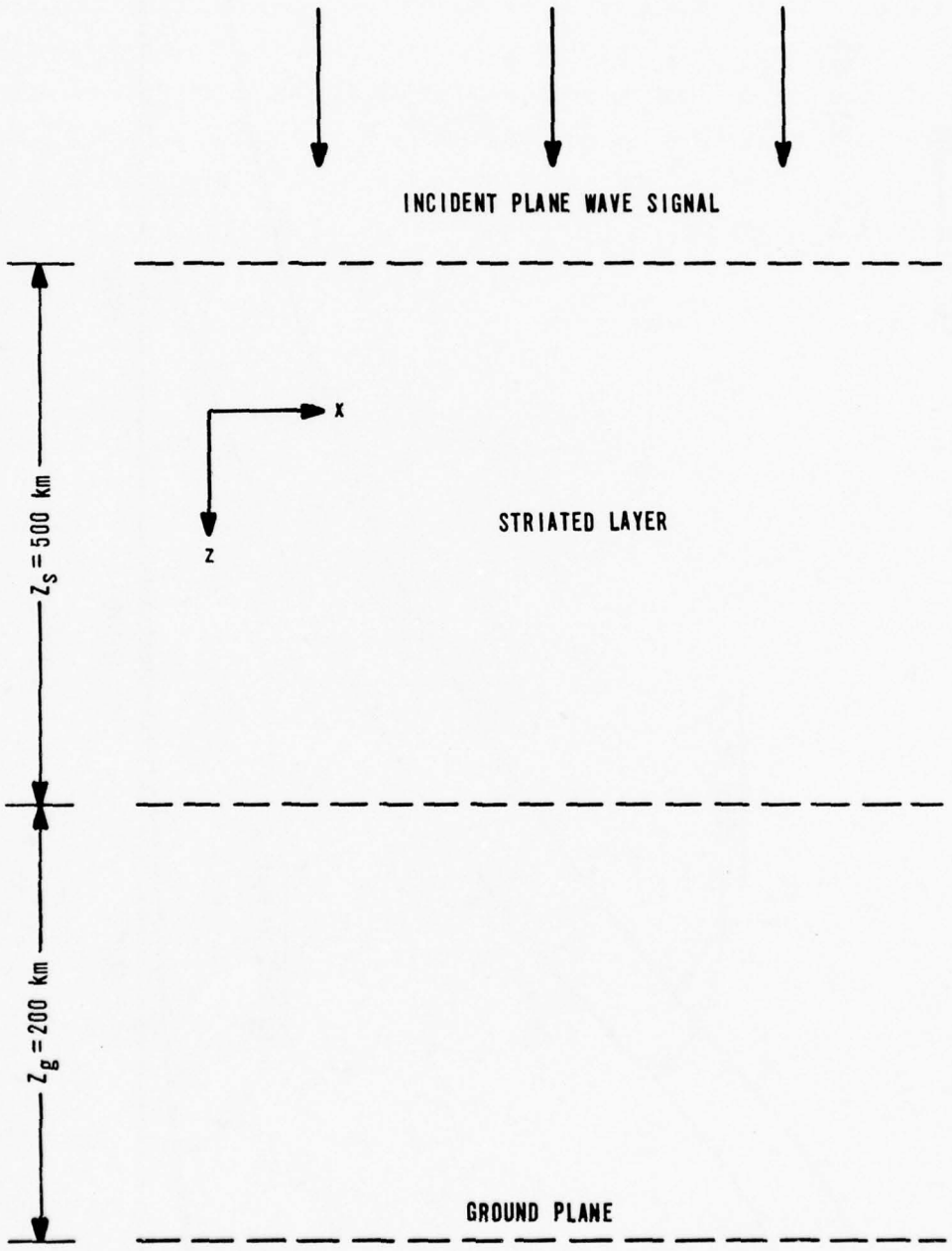

Figure 1. Propagation Geometry.

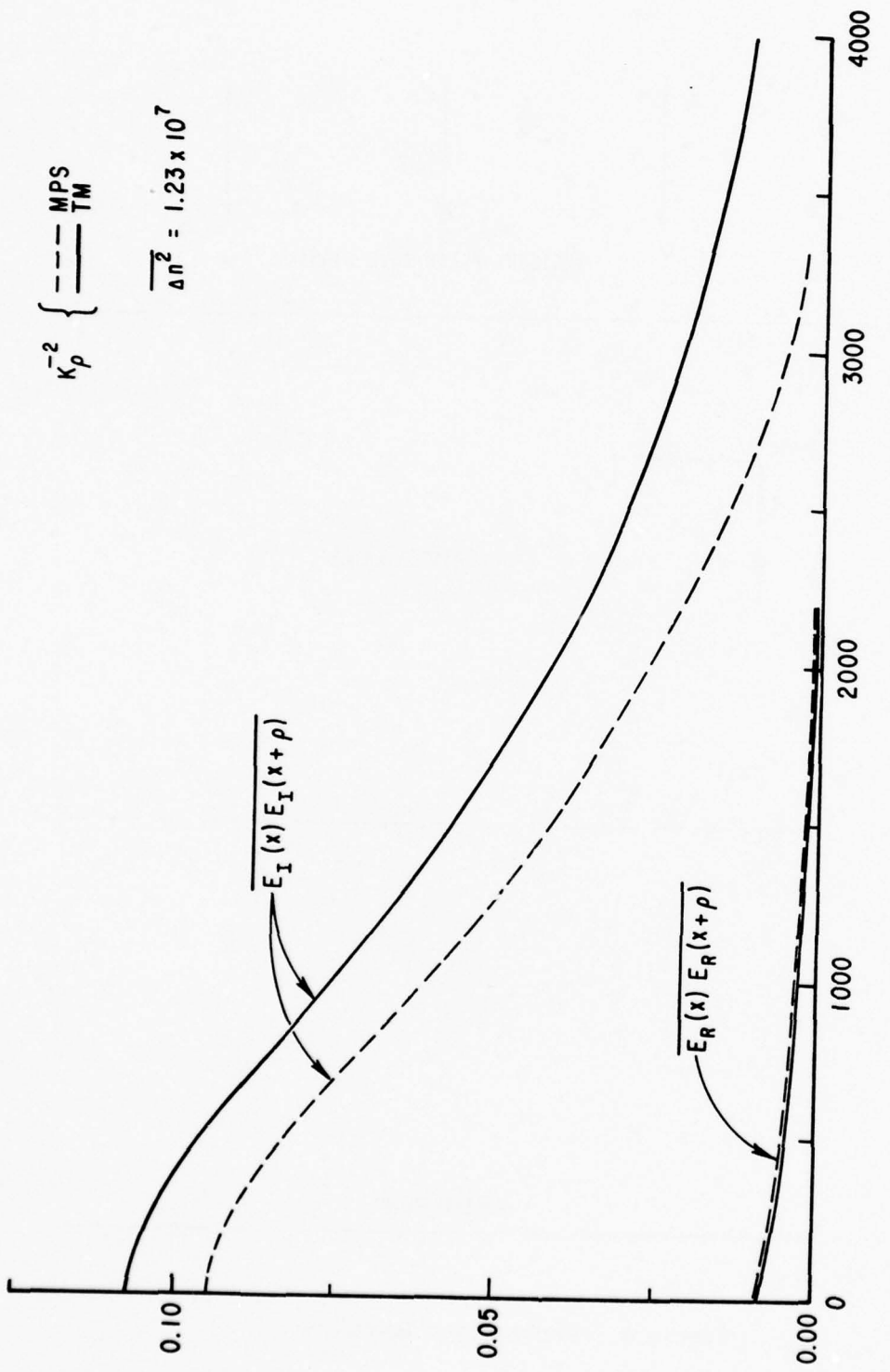

Figure 2. Quadrature Component Correlation Functions for $\overline{\Delta n^2} = 1.23 \times 10^7$.

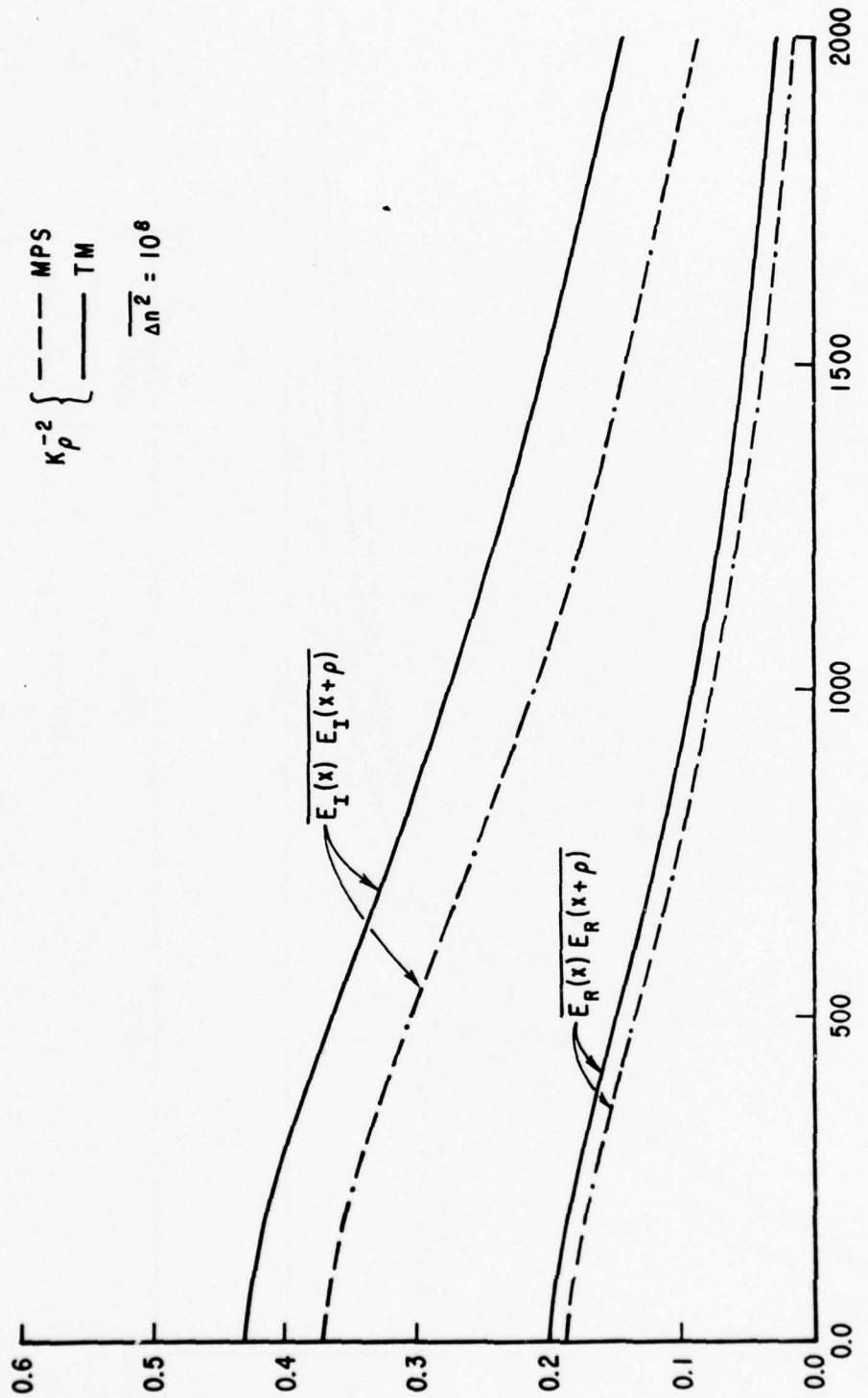

Figure 3. Quadrature Component Correlation Functions for $\overline{\Delta n^2} = 10^8$.

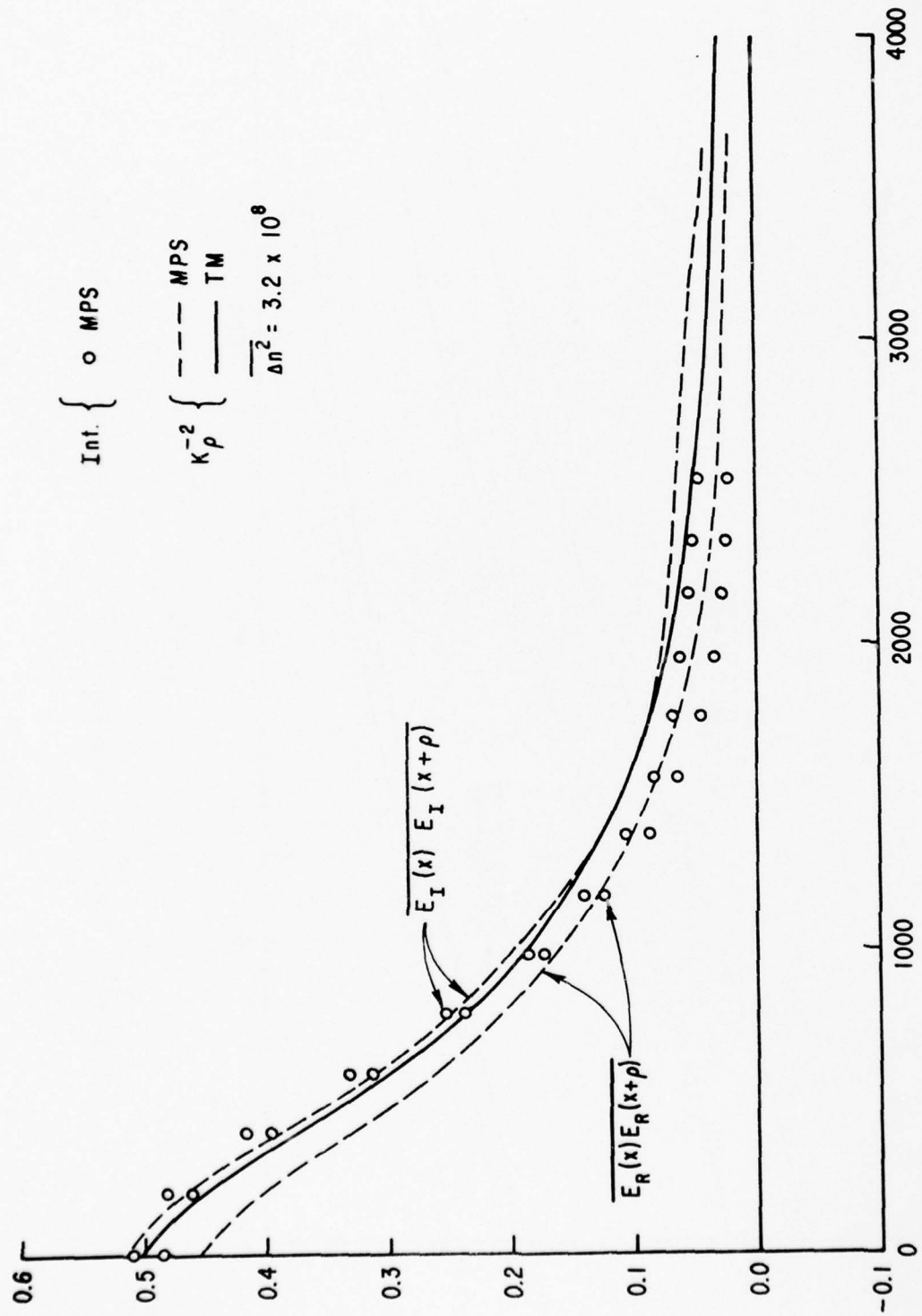

Figure 4. Quadrature Component Correlation Functions for $\overline{\Delta n^2} = 3.2 \times 10^8$.

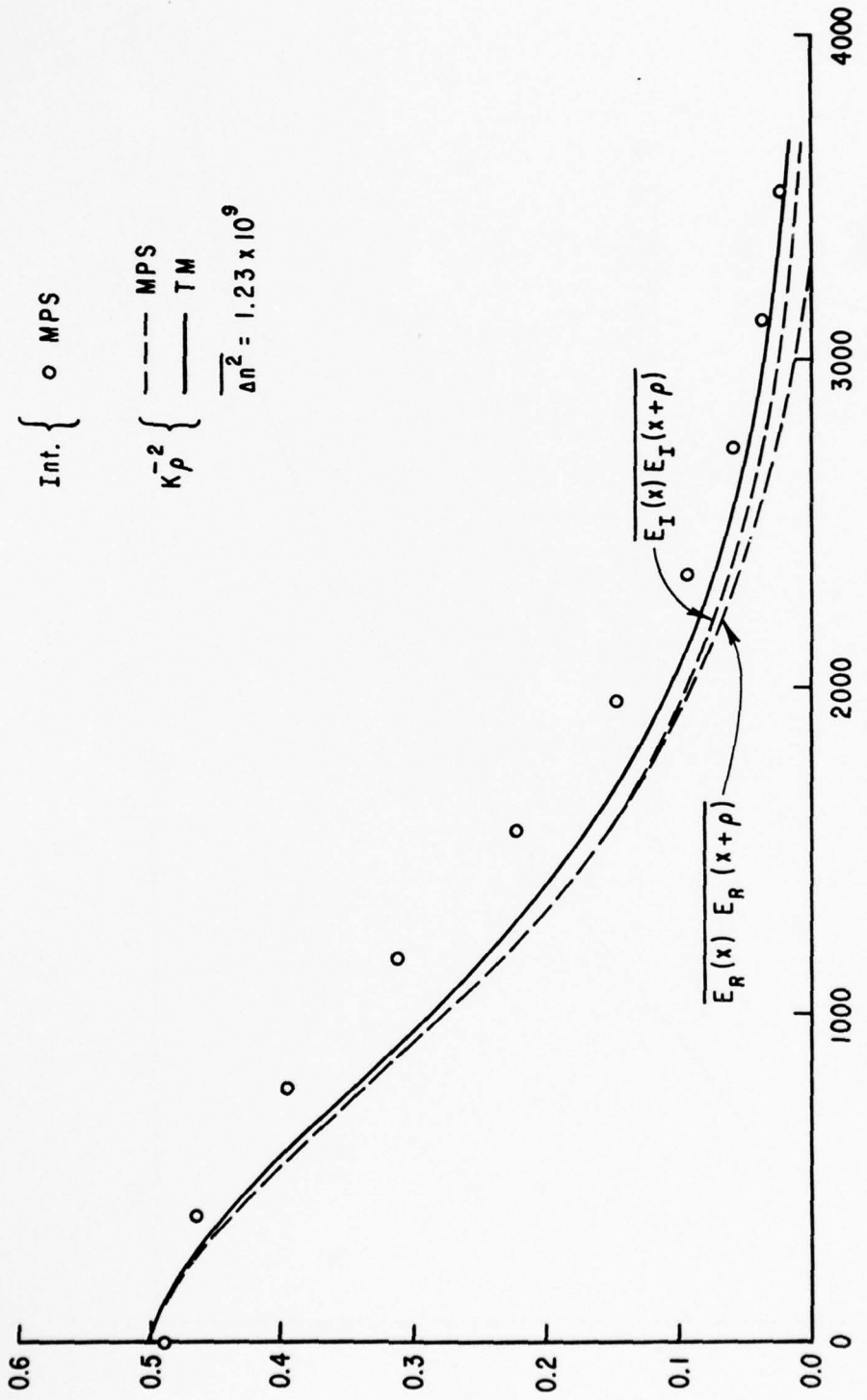

Figure 5. Quadrature Component Correlation Functions for $\overline{\Delta n^2} = 1.23 \times 10^9$.

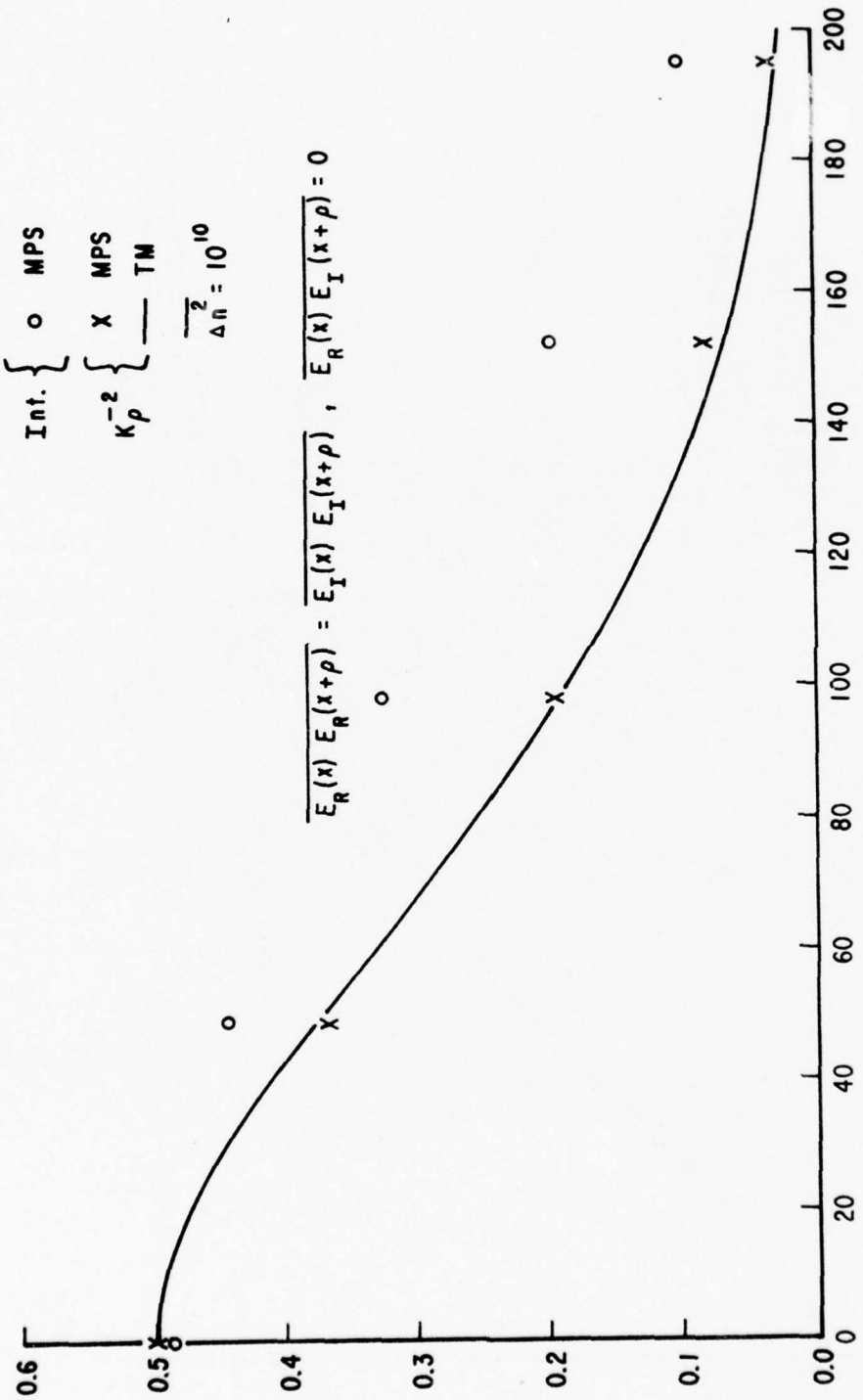

Figure 6. Quadrature Component Correlation Functions for $\overline{\Delta n^2} = 10^{10}$.

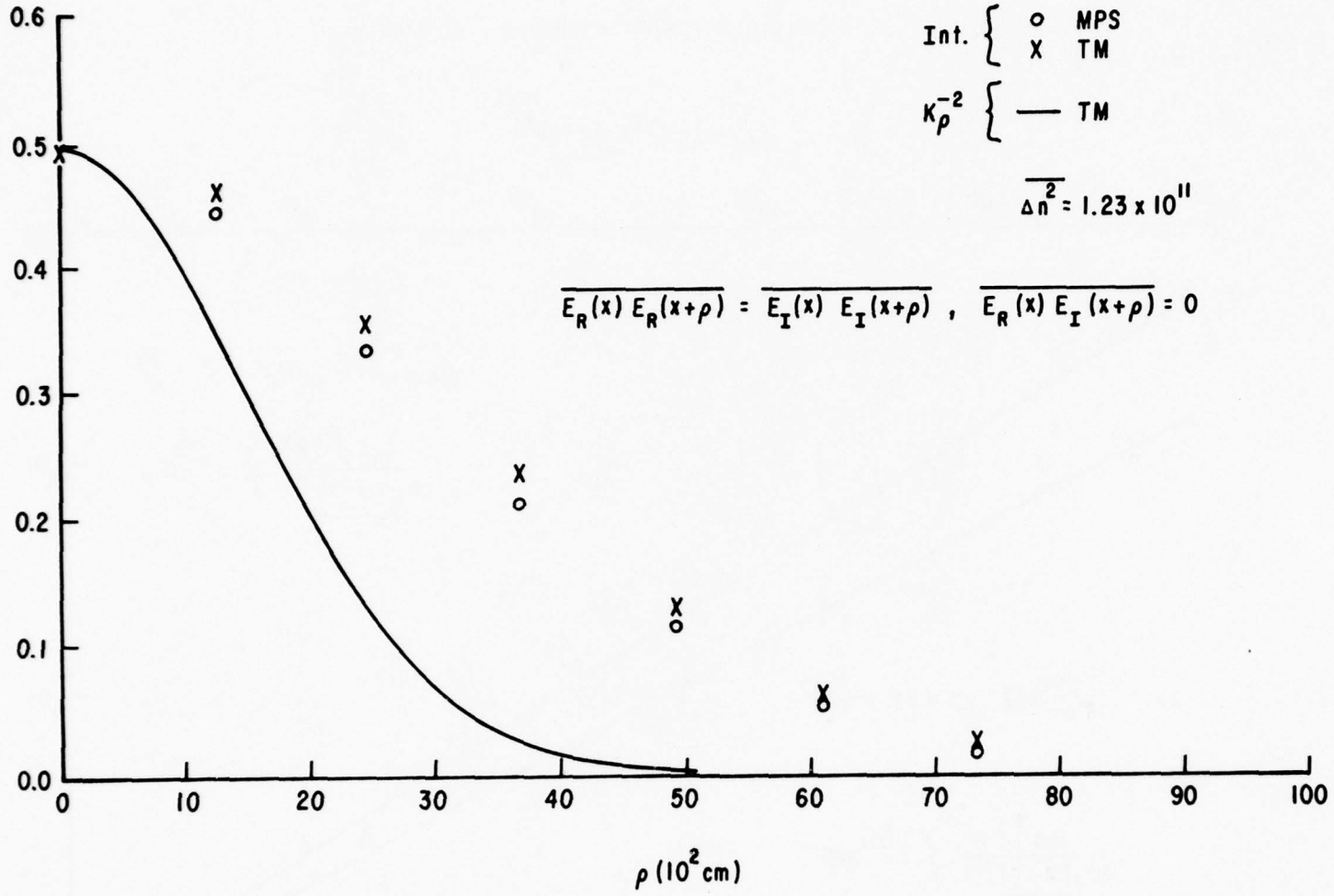

Figure 7. Quadrature Component Correlation Functions for $\overline{\Delta n^2} = 1.23 \times 10^{11}$.

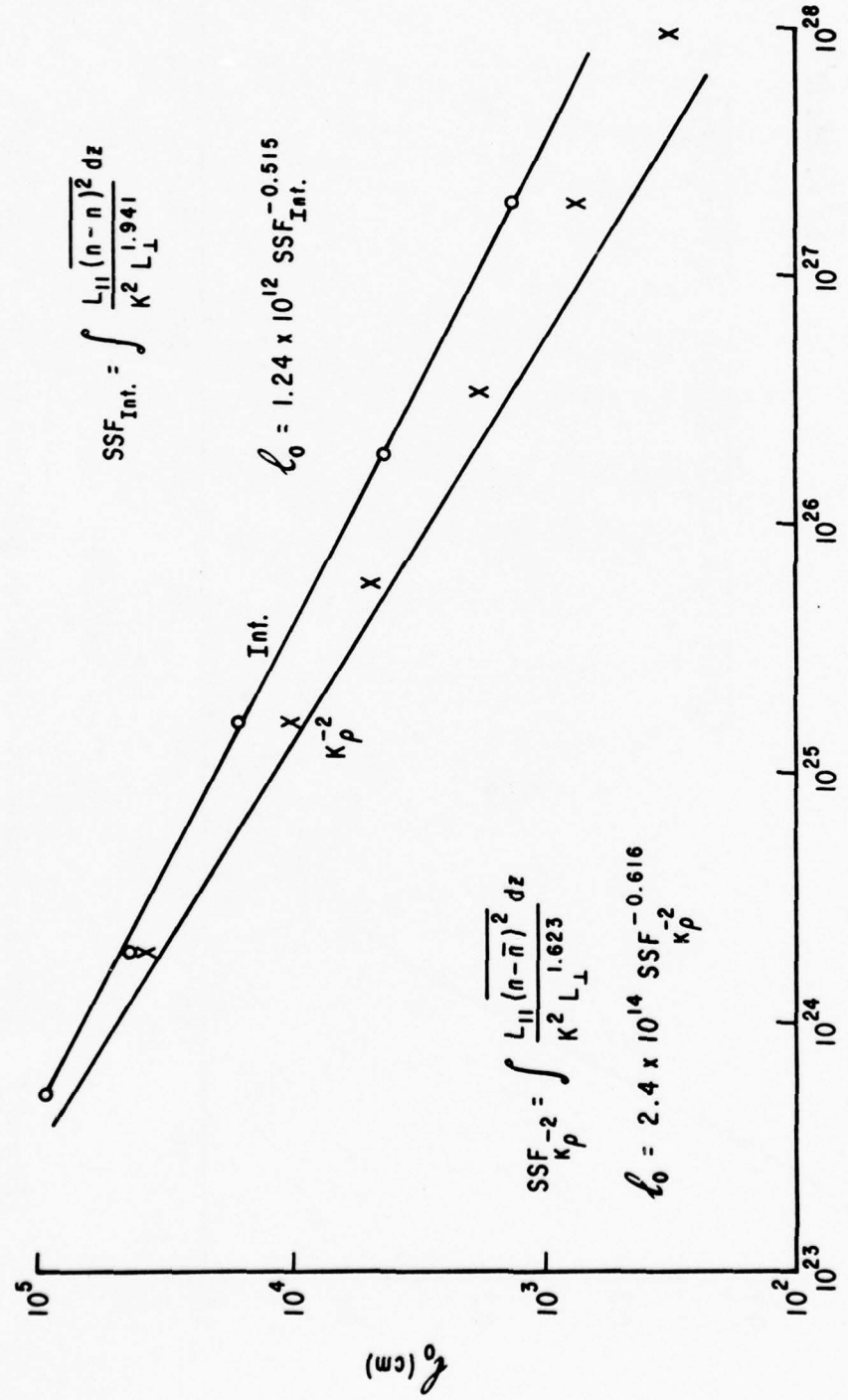

Figure 8. Field Correlation Distance (ℓ_o).

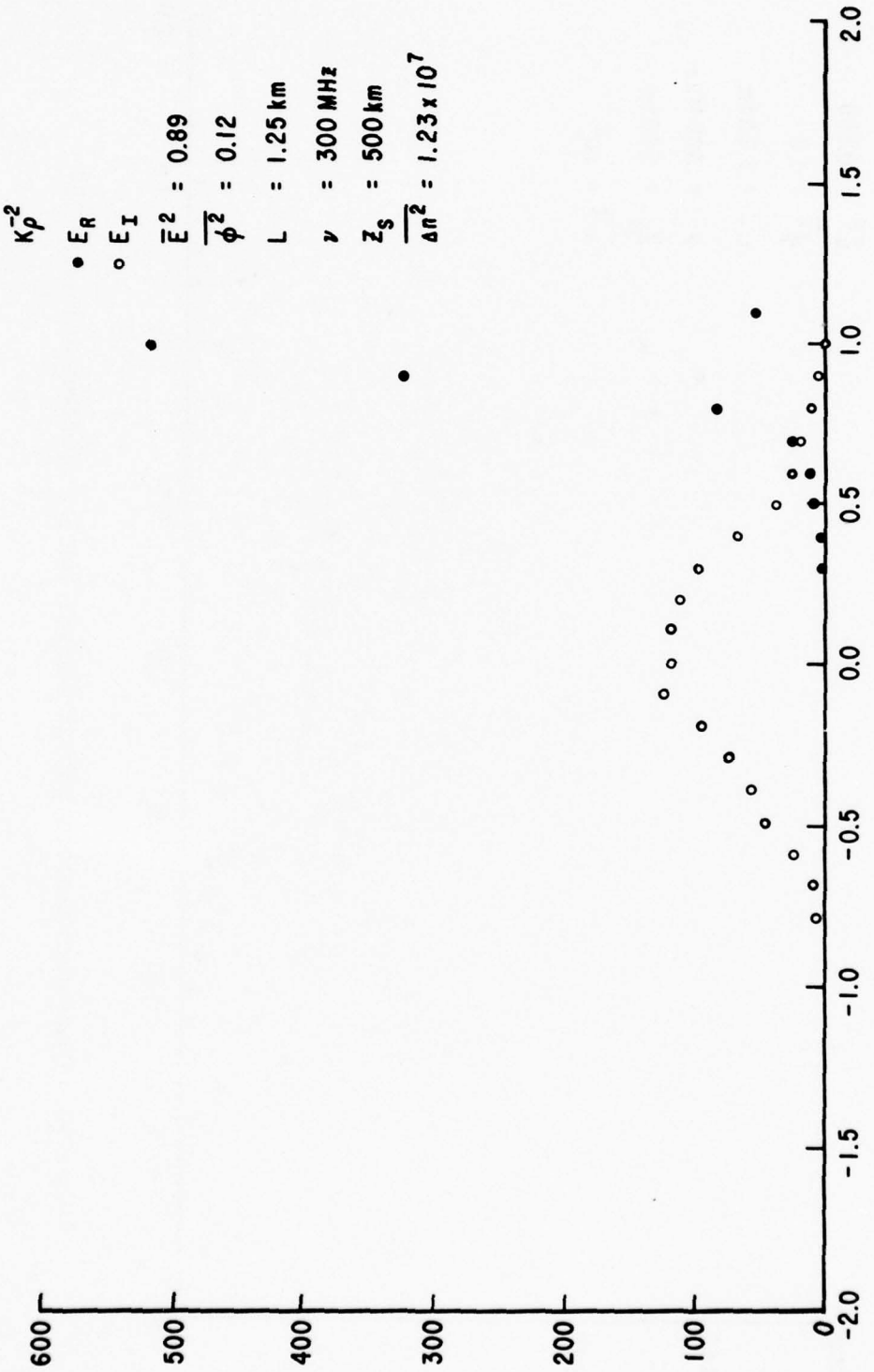

Figure 9. Quadrature Component Distributions for K_ρ^{-2} Spectrum and $\overline{\Delta n^2}$ = 1.23 x 10^7.

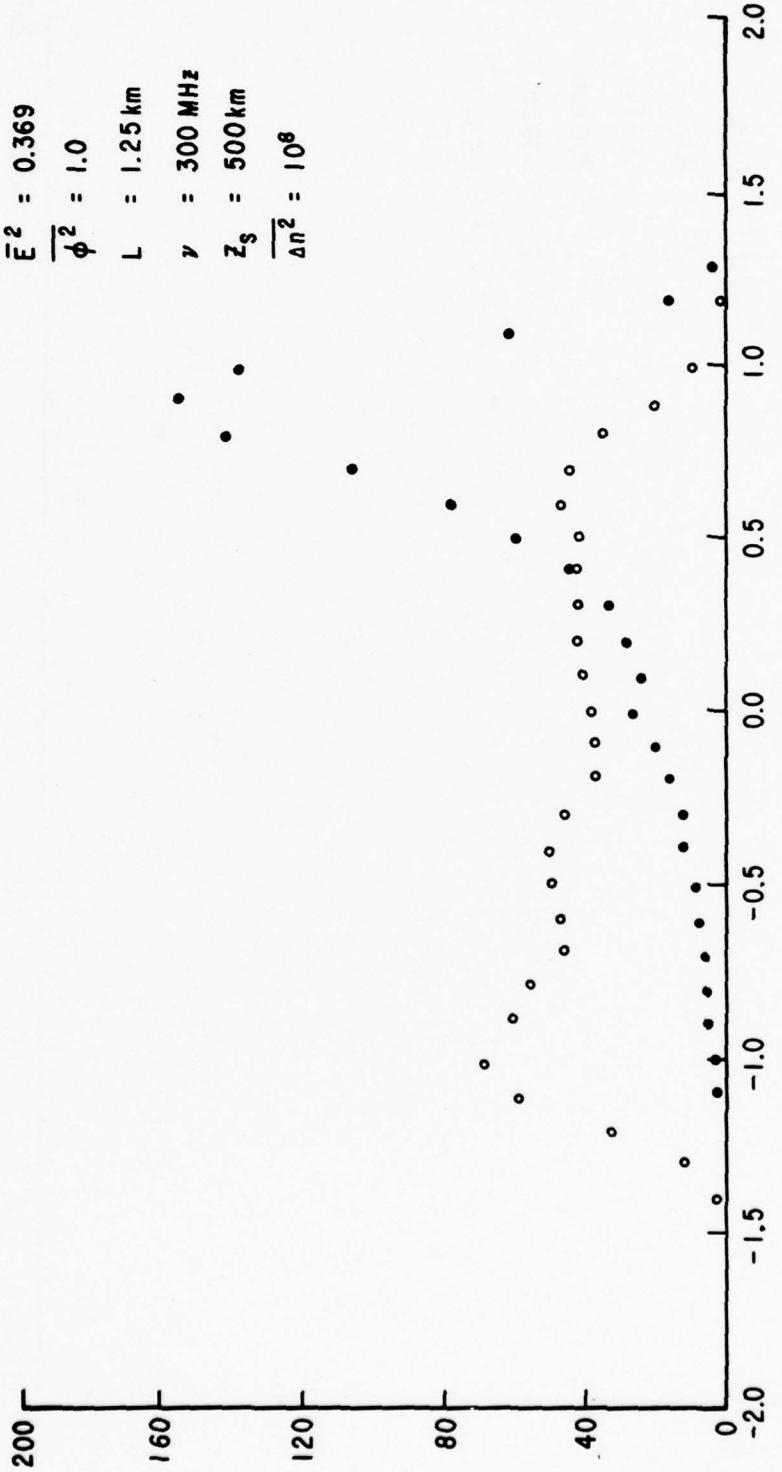

Figure 10. Quadrature Component Distributions for K_ρ^{-2} Spectrum and $\overline{\Delta n^2} = 10^8$.

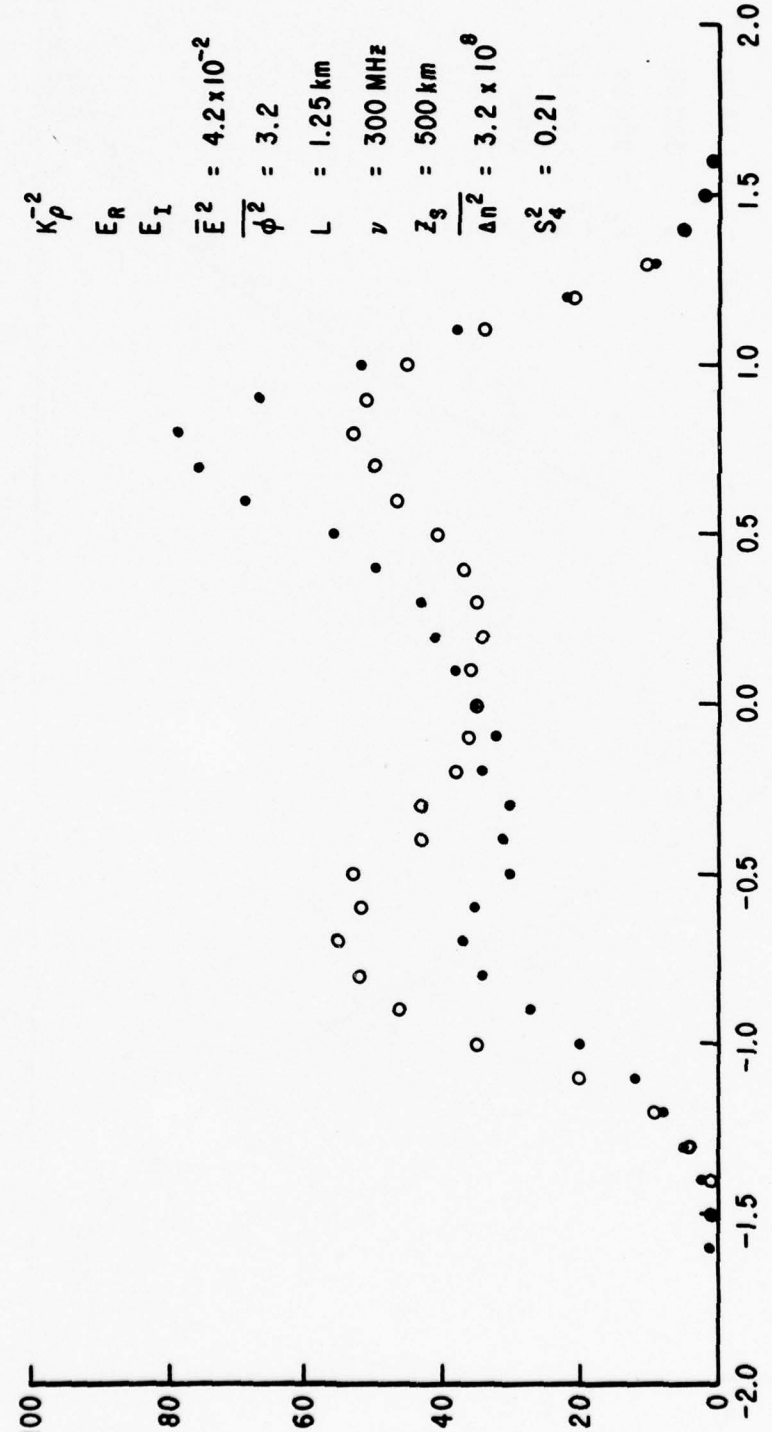

Figure 11. Quadrature Component Distributions for K_ρ^{-2} Spectrum and $\overline{\Delta n^2}$ = 3.2 x 10^8.

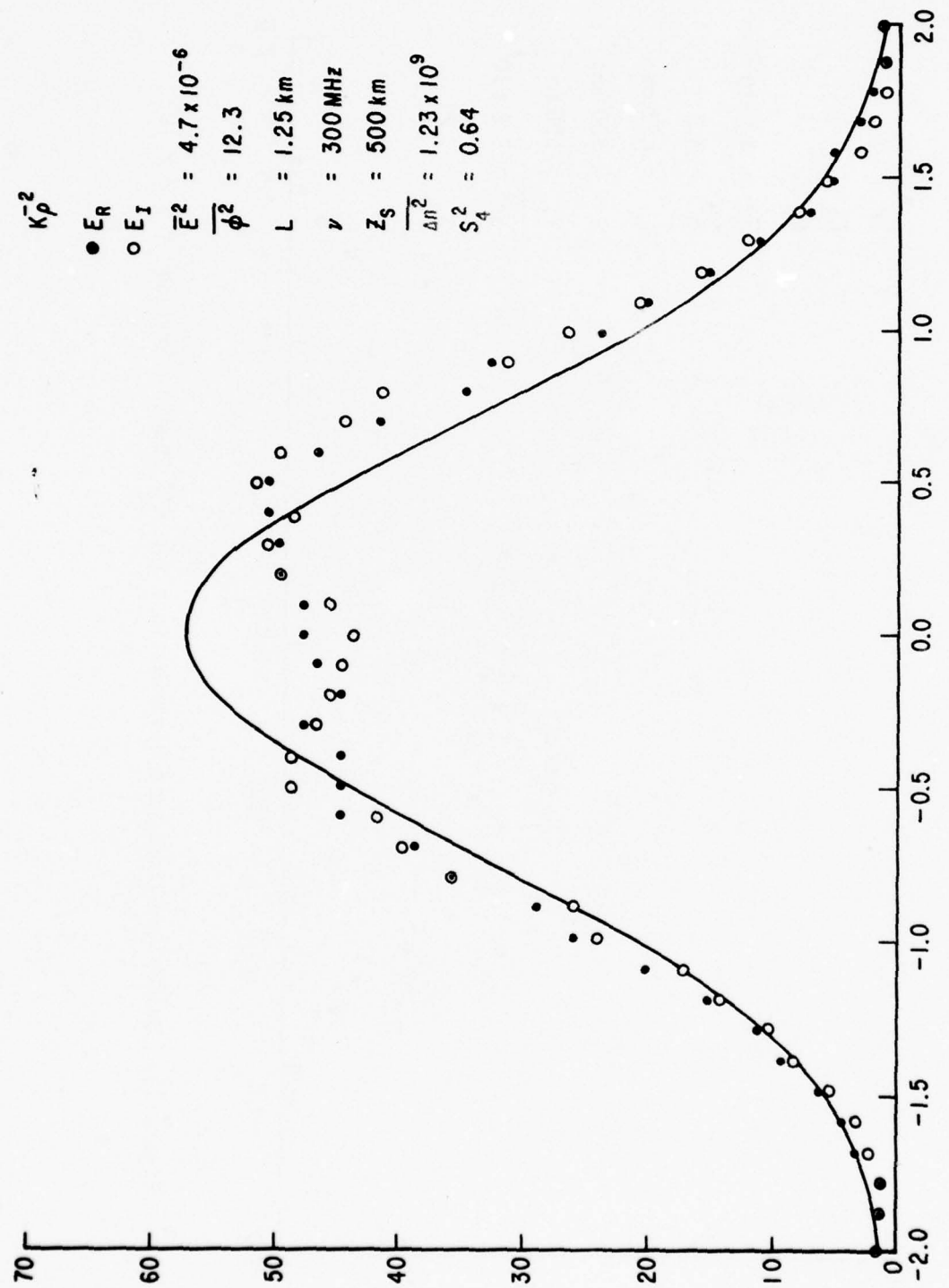

Figure 12. Quadrature Component Distributions for K_ρ^{-2} Spectrum and $\overline{\Delta n^2} = 1.23 \times 10^9$.

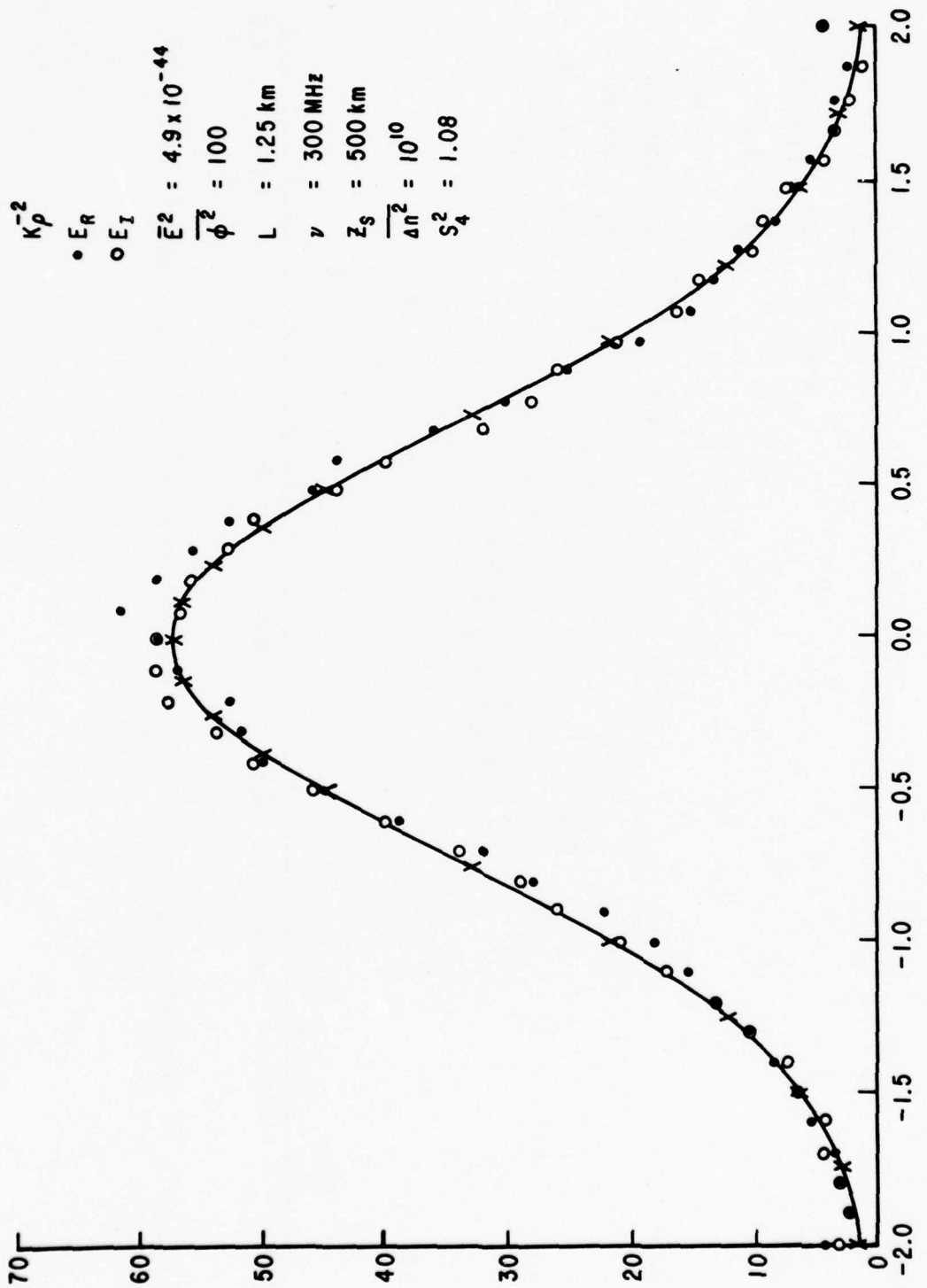

Figure 13. Quadrature Component Distributions for K_ρ^{-2} Spectrum and $\overline{\Delta n^2} = 10^{10}$.

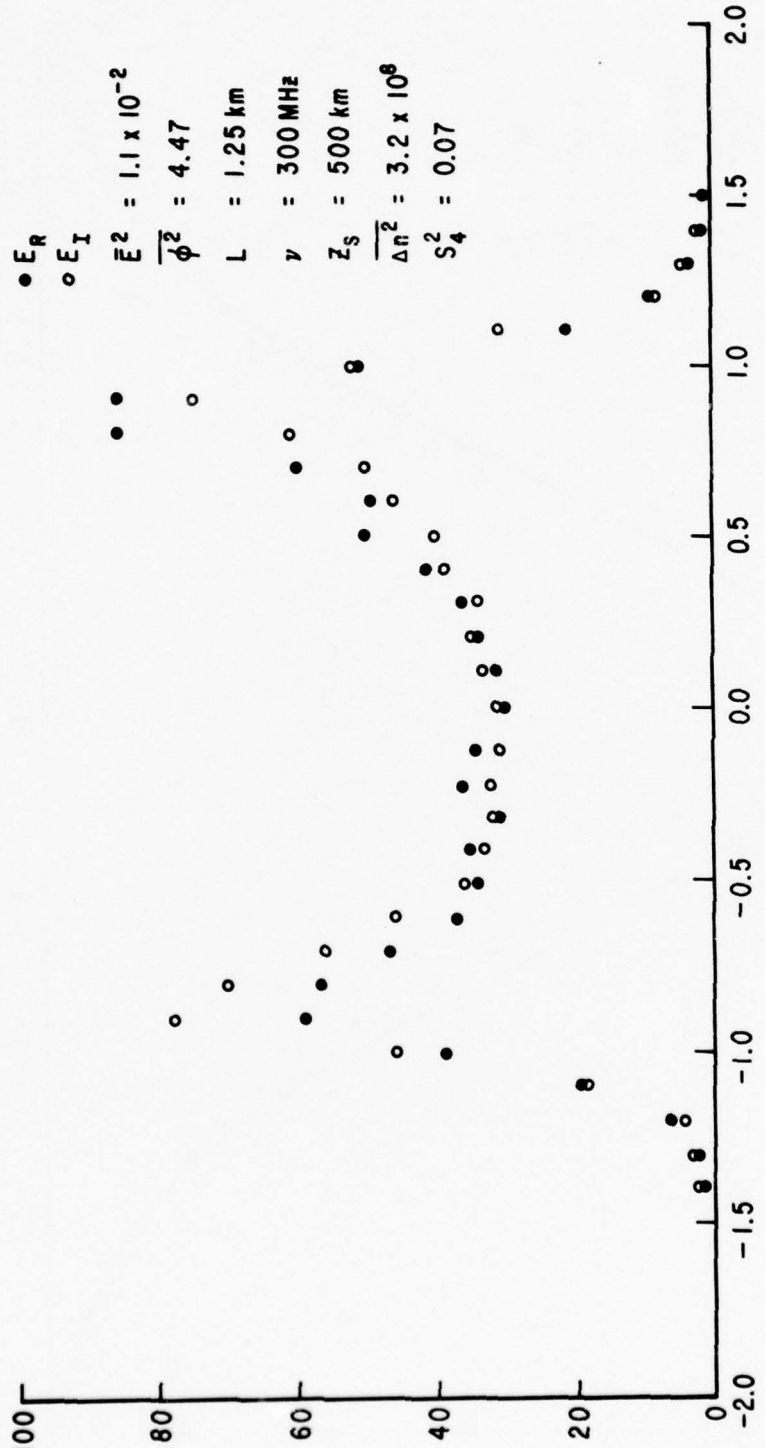

Figure 14. Quadrature Component Distributions for Intermediate Specturm and $\overline{\Delta n^2}$ = 3.2 x 10^8.

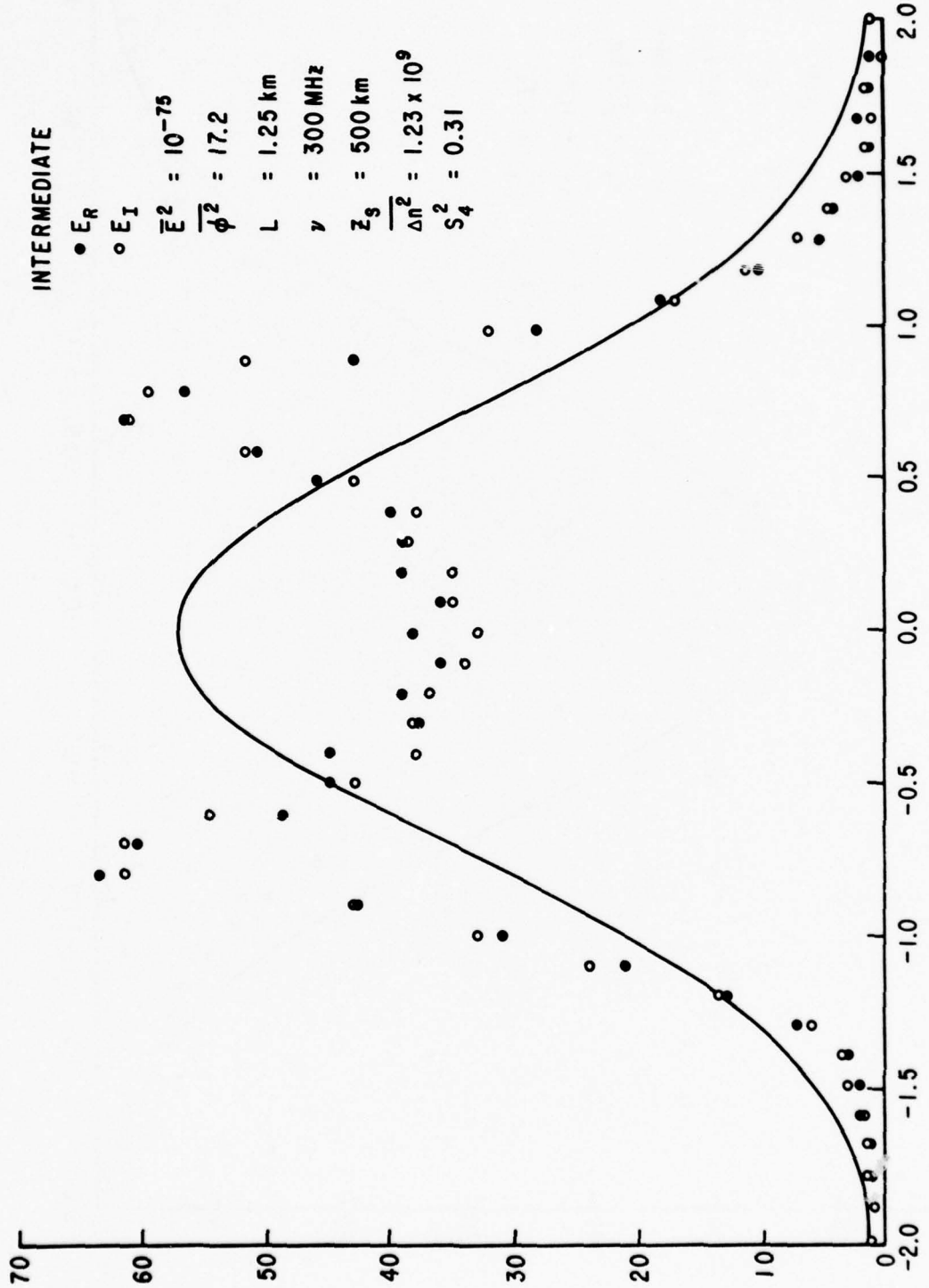

Figure 15. Quadrature Component Distributions for Intermediate Spectrum and $\overline{\Delta n^2}$ = 1.23 x 10^9.

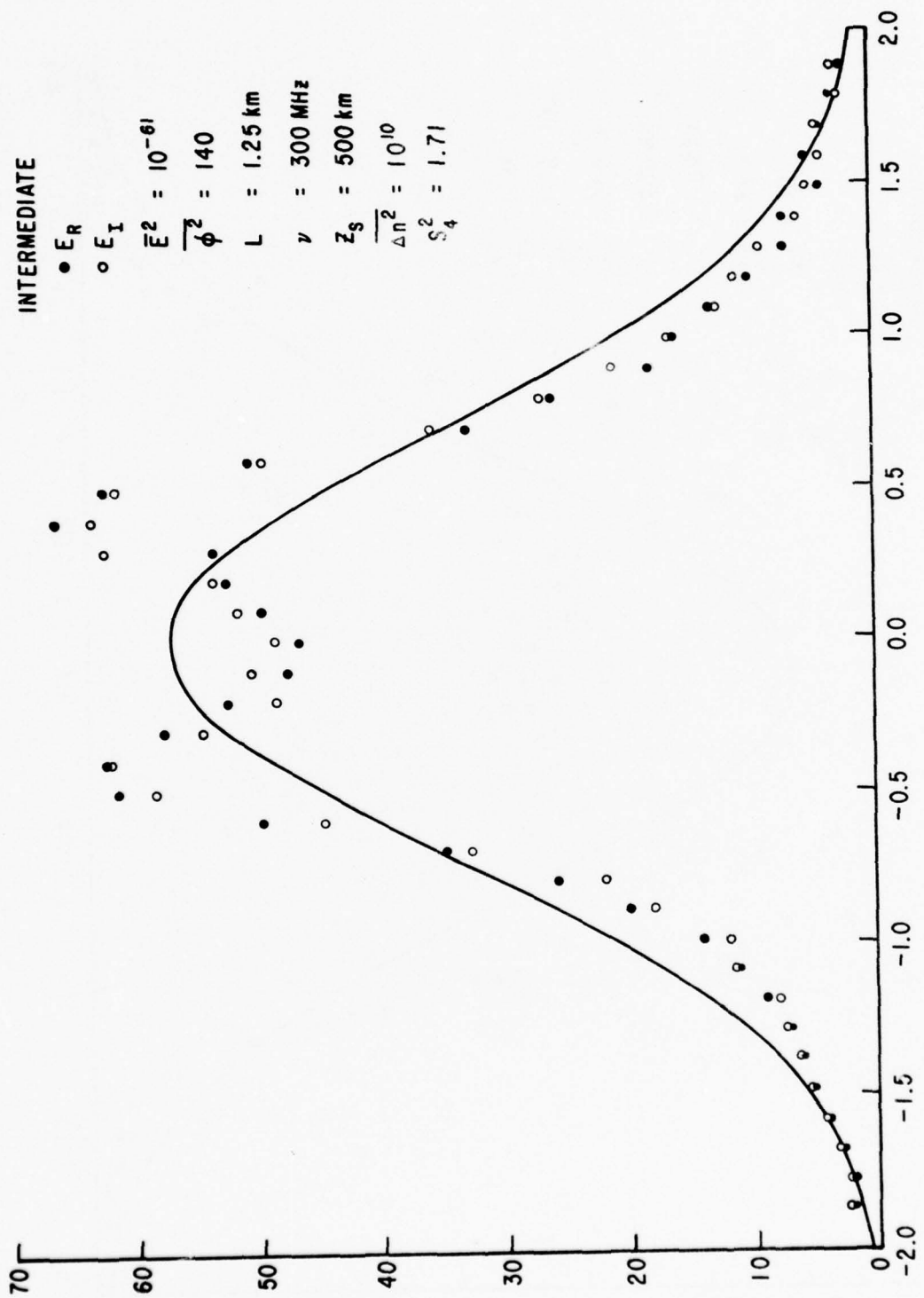

Figure 16. Quadrature Component Distributions for Intermediate Spectrum and $\overline{\Delta n^2} = 10^{10}$.

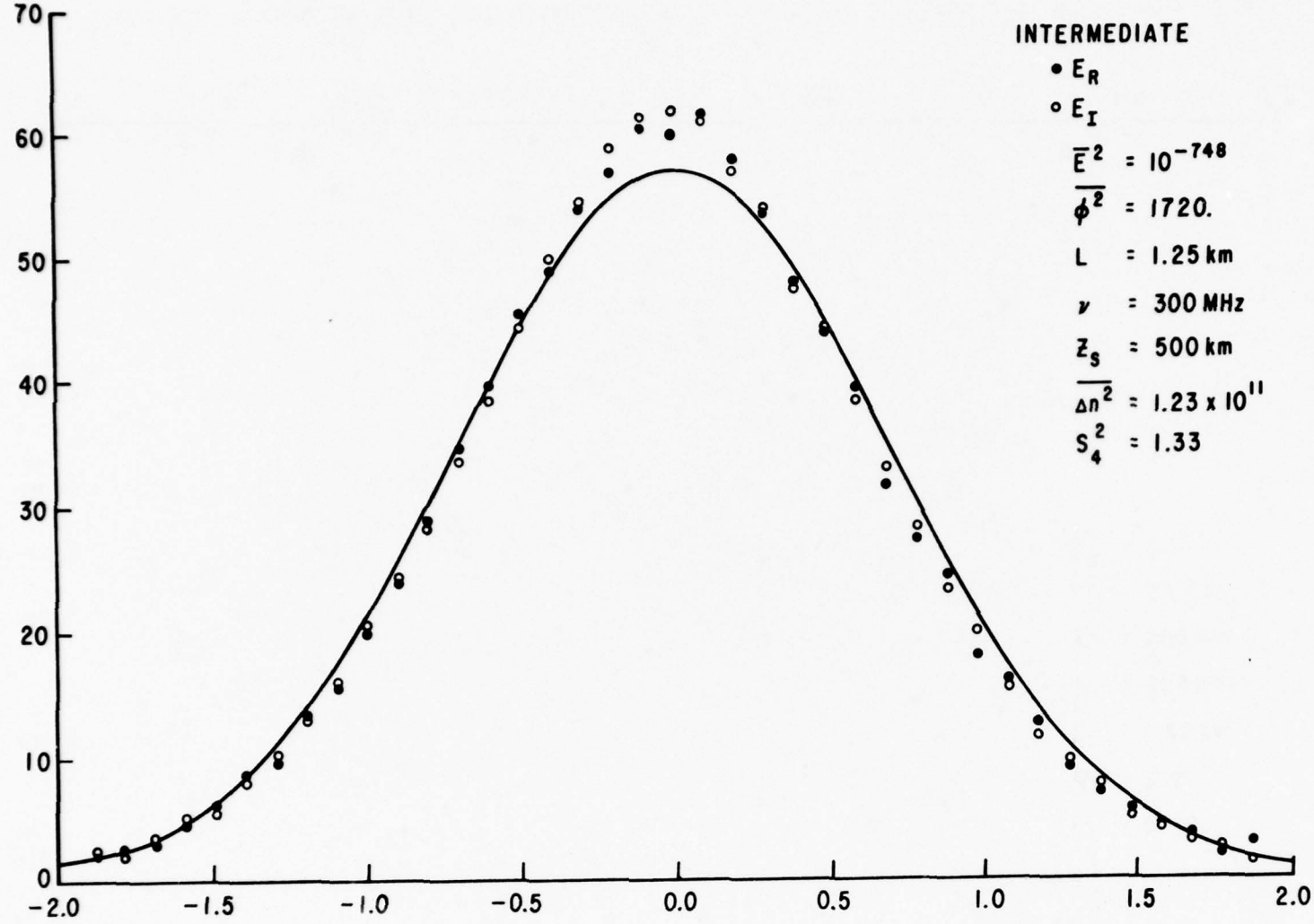

Figure 17. Quadrature Component Distributions for Intermediate Spectrum and $\overline{\Delta n^2} = 1.23 \times 10^{11}$.

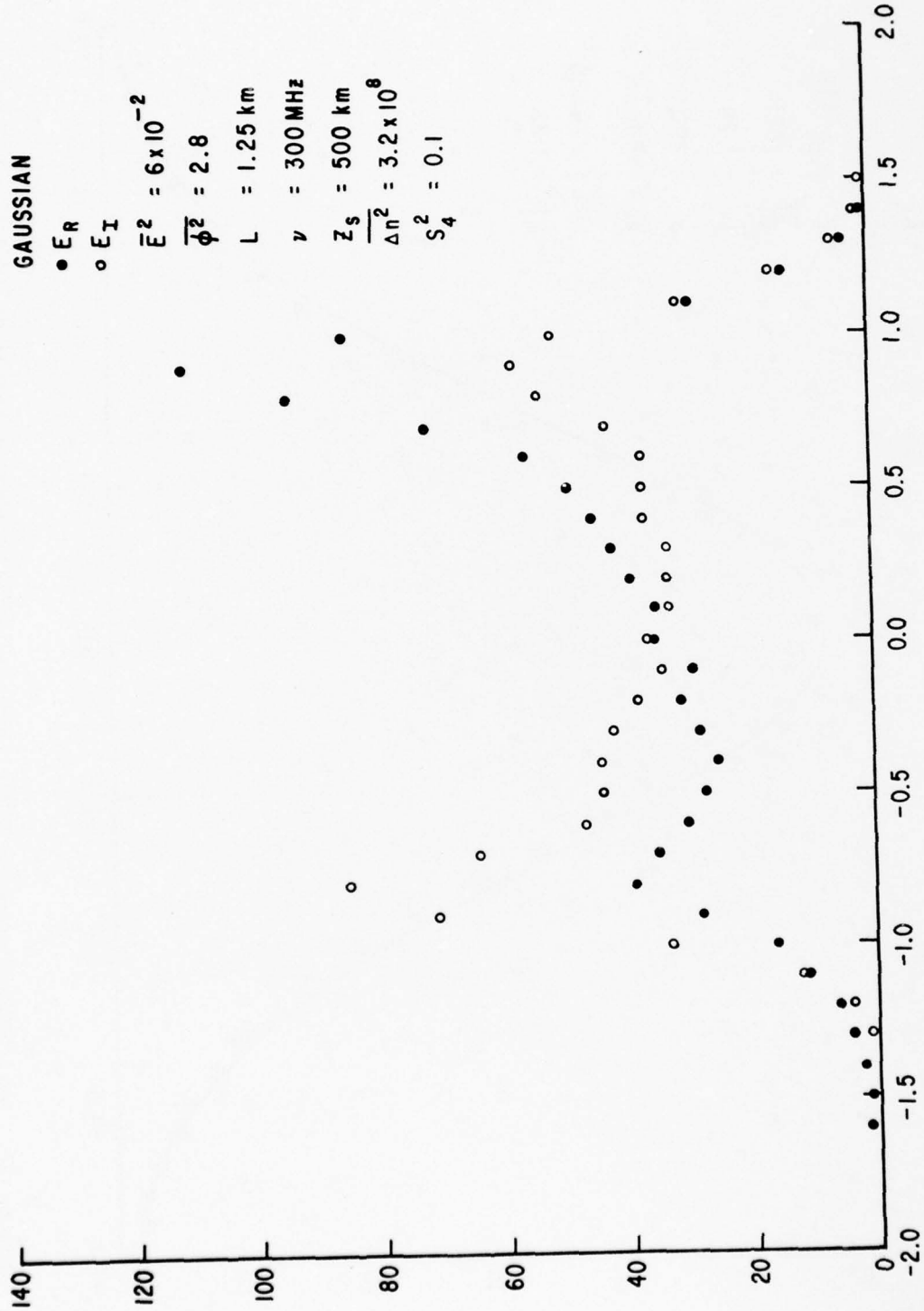

Figure 18. Quadrature Component Distributions for Gaussian Spectrum and $\overline{\Delta n^2} = 3.2 \times 10^8$.

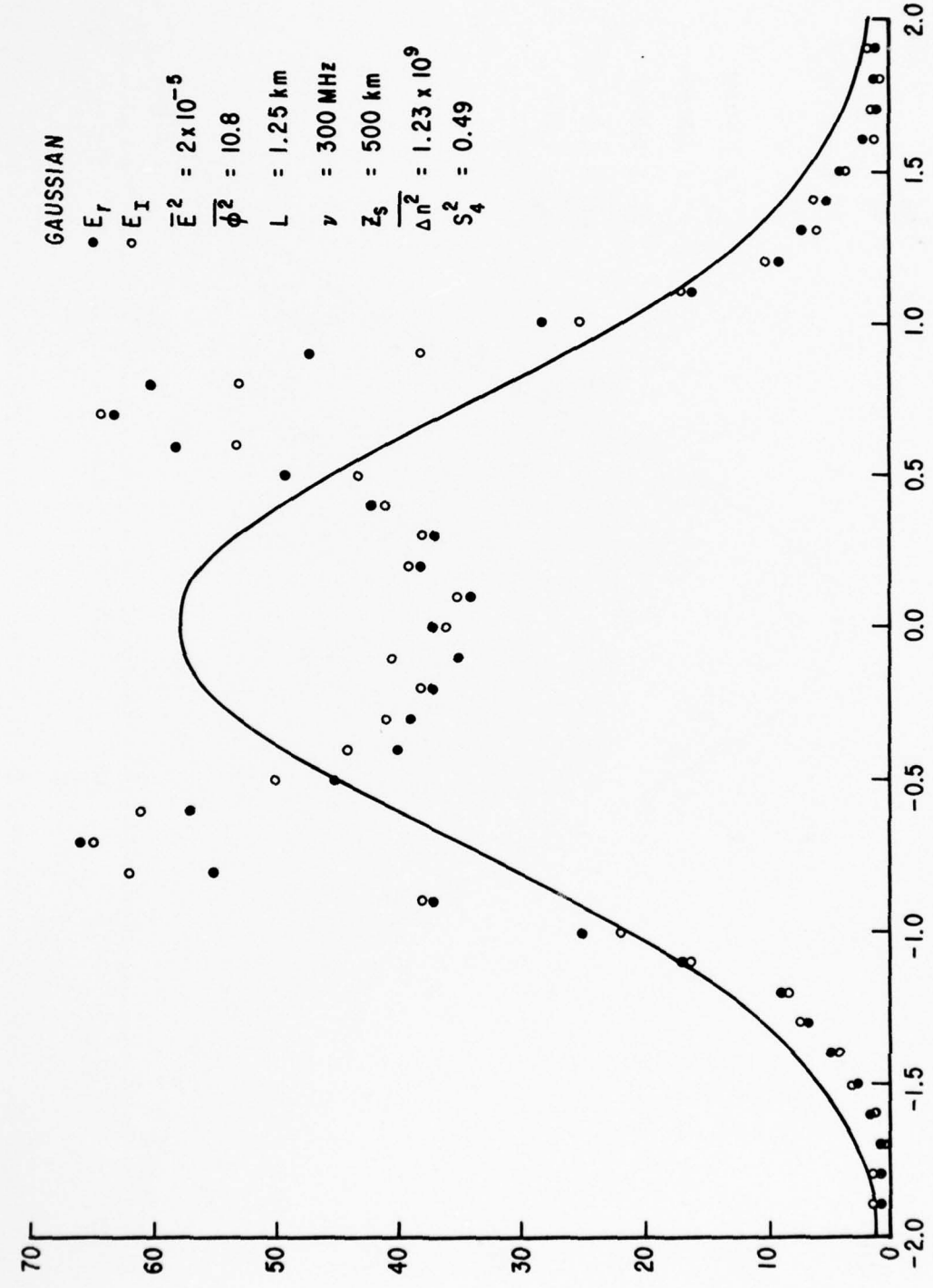

Figure 19. Quadrature Component Distributions for Gaussian Spectrum and $\overline{\Delta n^2}$ = 1.23 x 10^9.

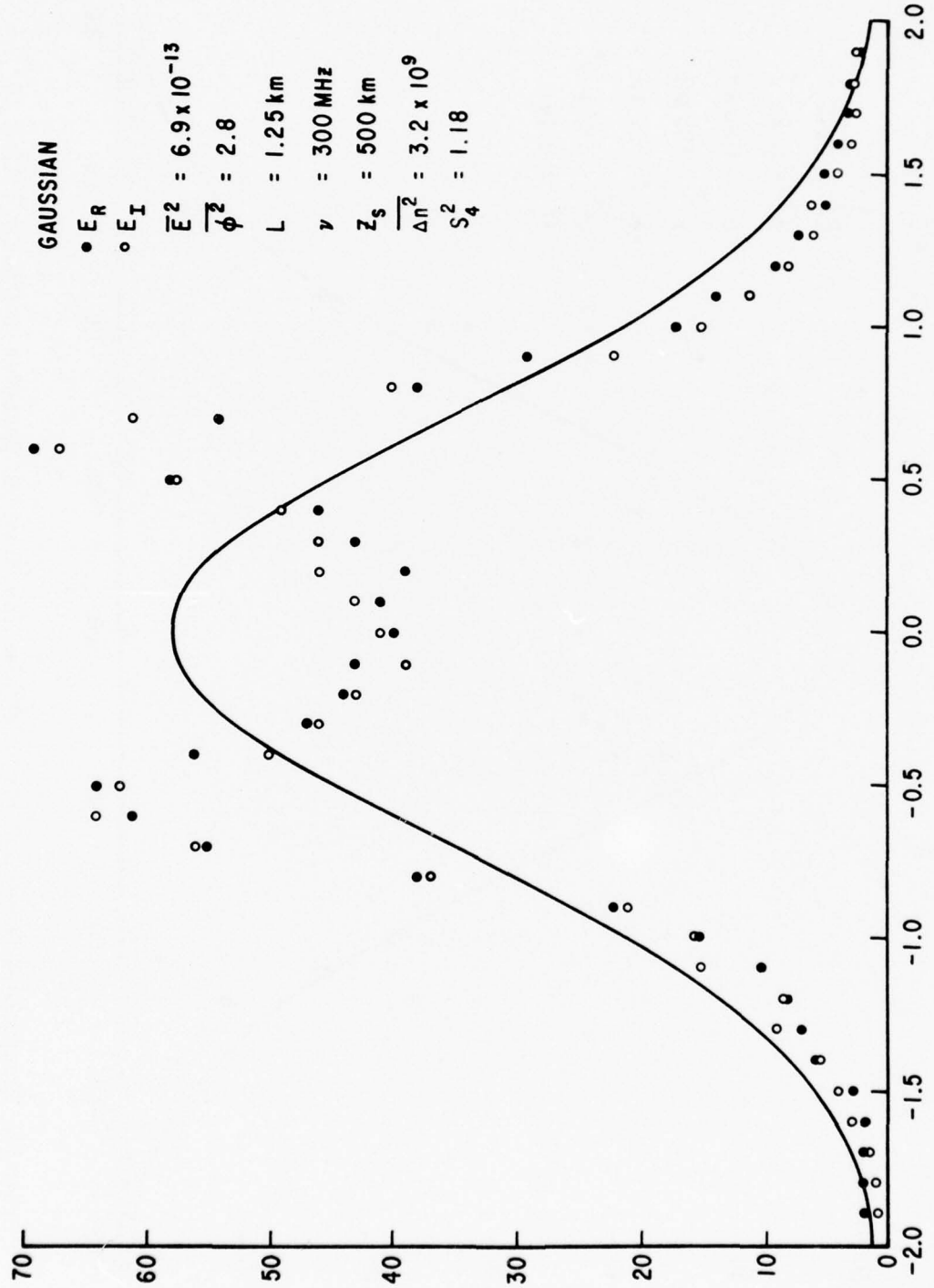

Figure 20. Quadrature Component Distributions for Guassian Spectrum and $\overline{\Delta n^2} = 3.2 \times 10^9$.

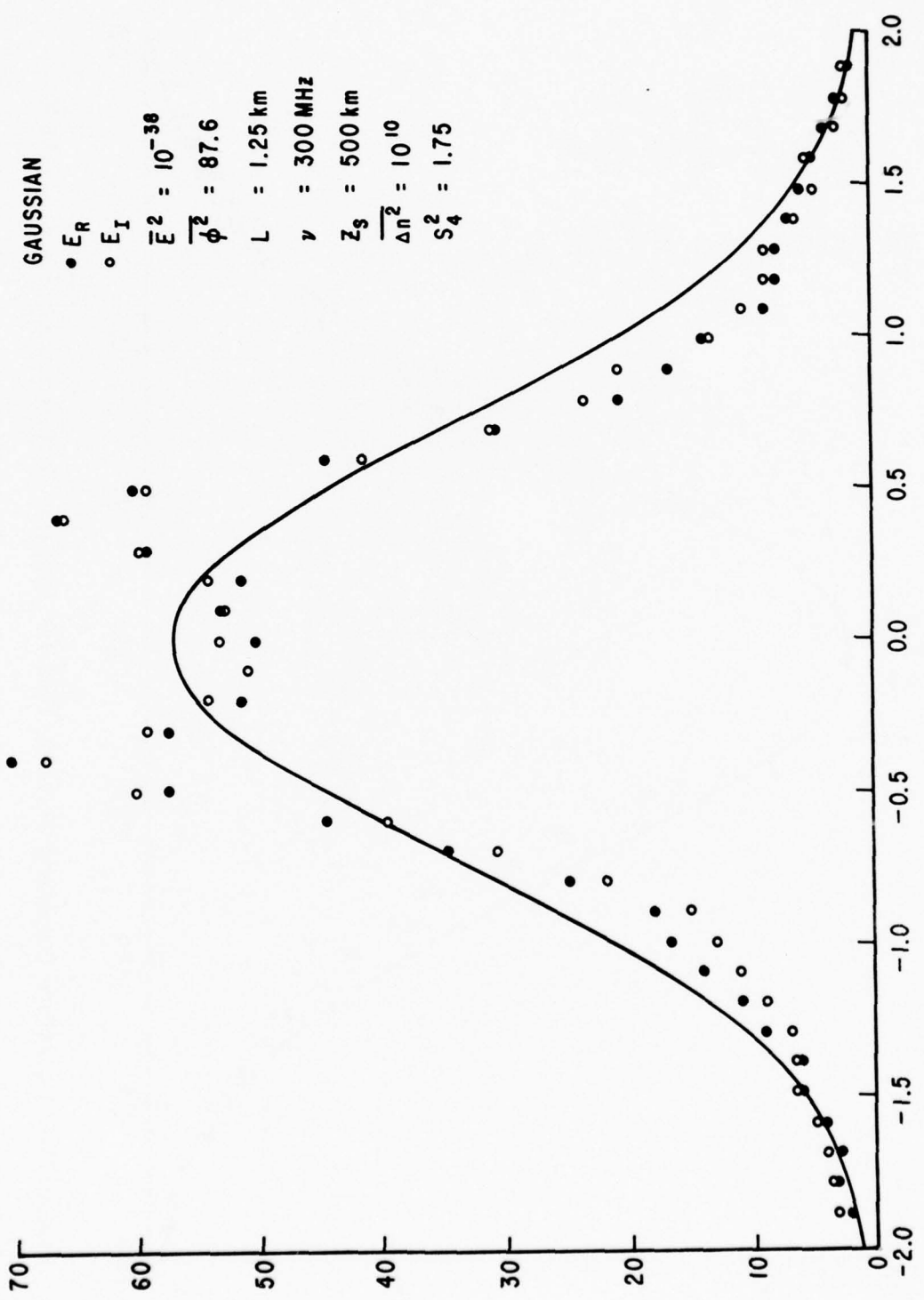

Figure 21. Quadrature Component Distributuions for Gaussian Spectrum and $\overline{\Delta n^2} = 10^{10}$.

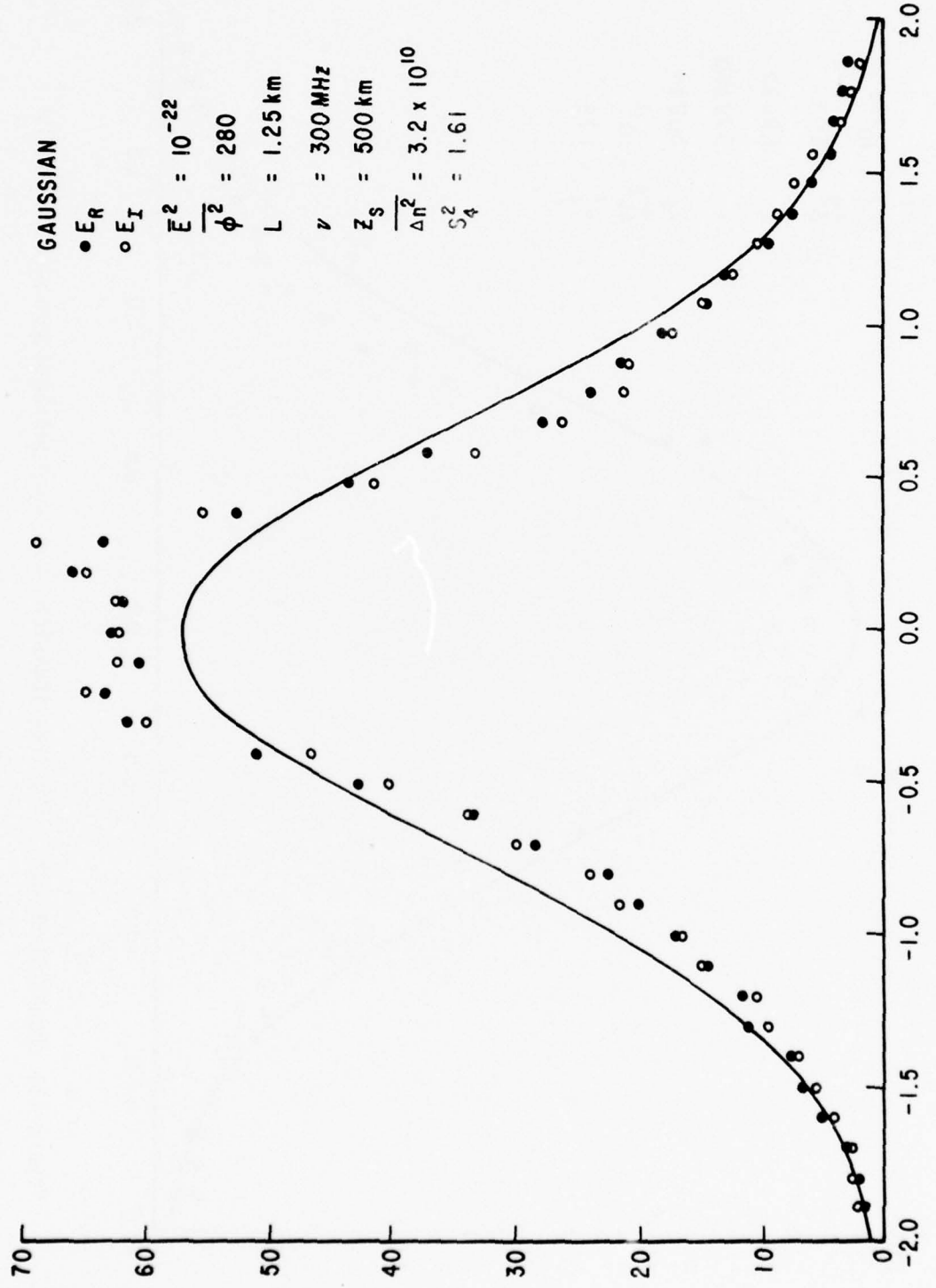

Figure 22. Quadrature Component Distributions for Gaussian Spectrum and $\overline{\Delta n^2}$ = 3.2 x 10^{10}.

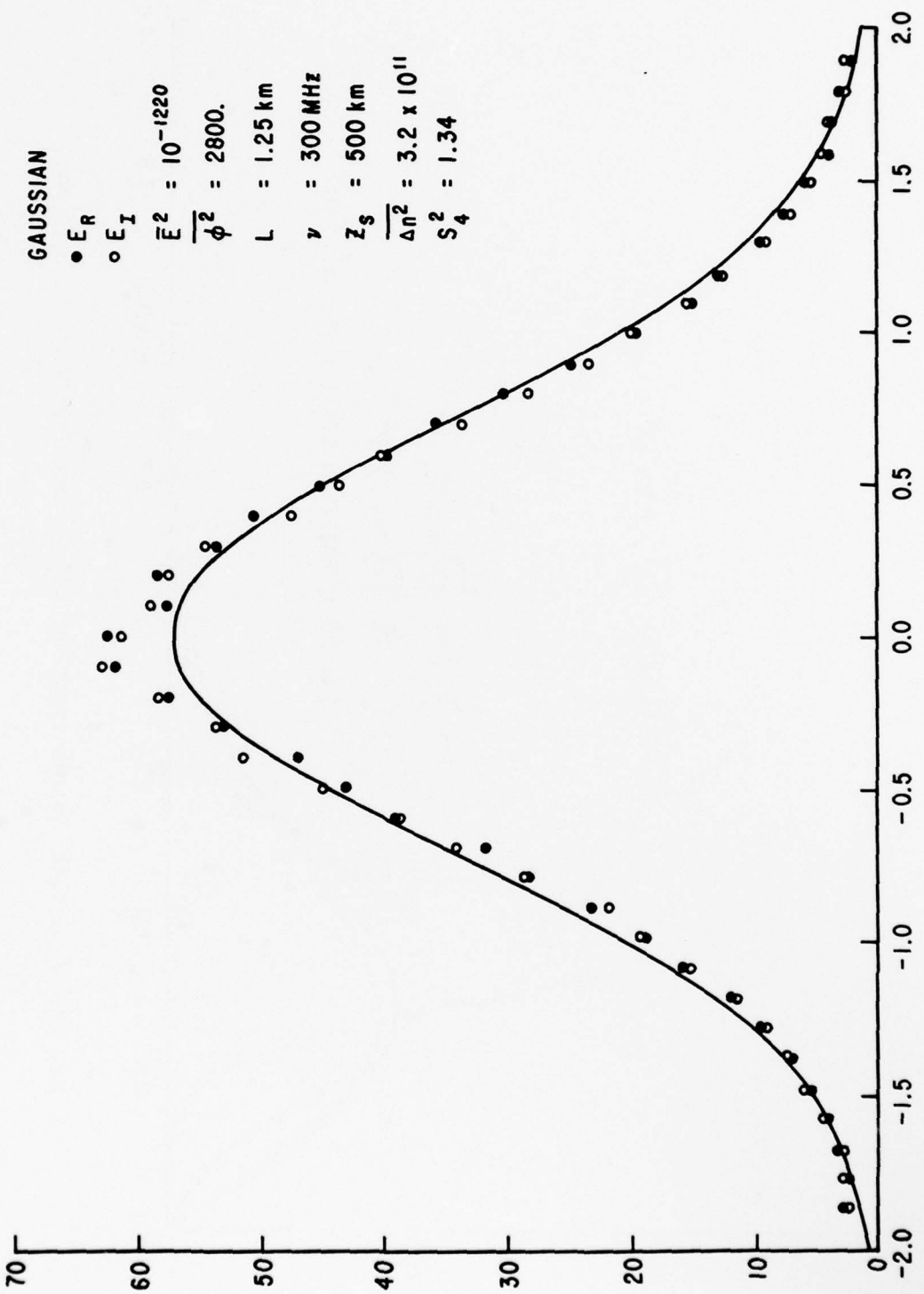

Figure 23. Quadrature Component Distributions for Gaussian Spectrum and $\overline{\Delta n^2}$ = 3.2 x 10^{11}.

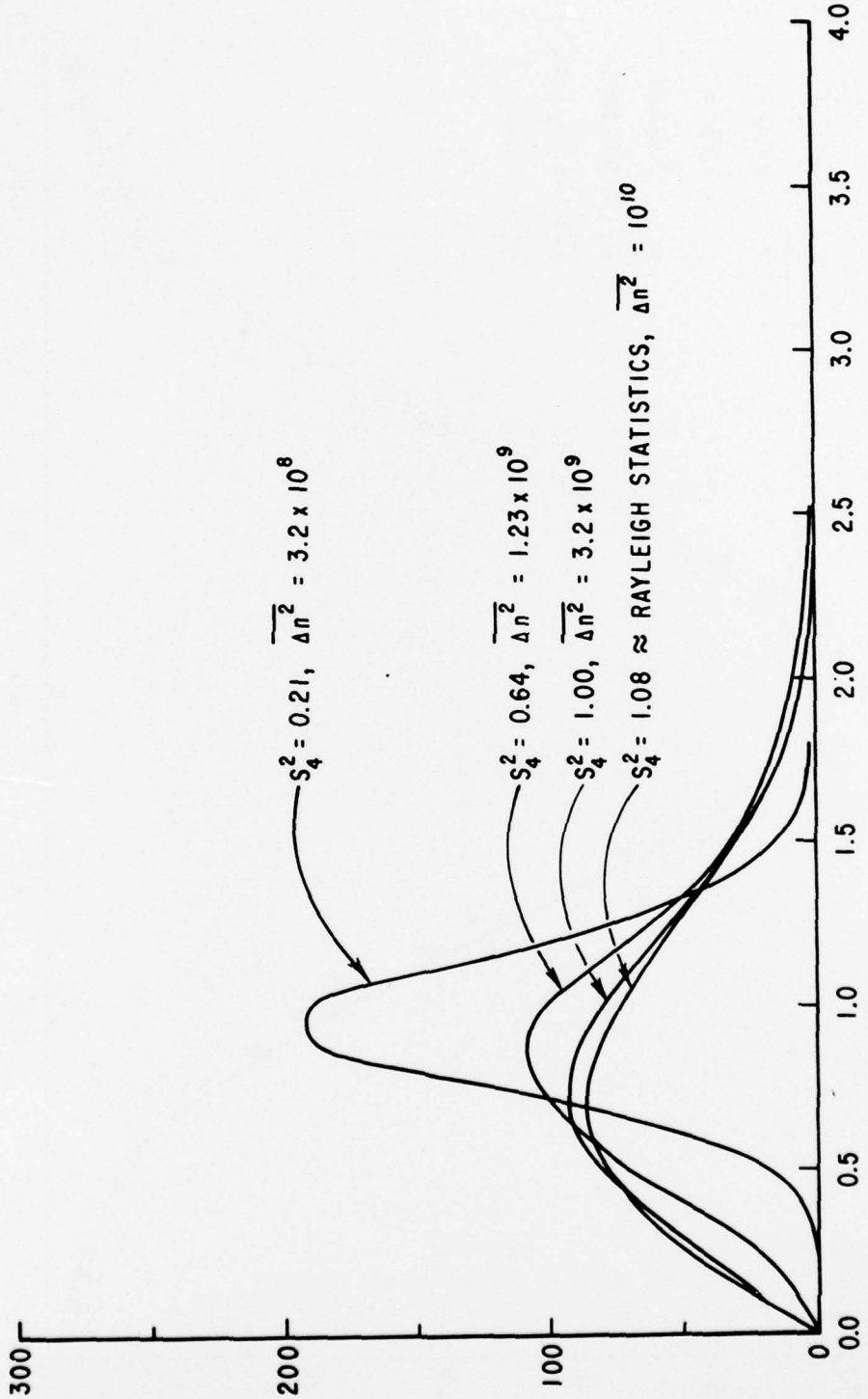

Figure 24. Amplitude Distributions for the K_ρ^{-2} Spectrum With L = 1.25 Km.

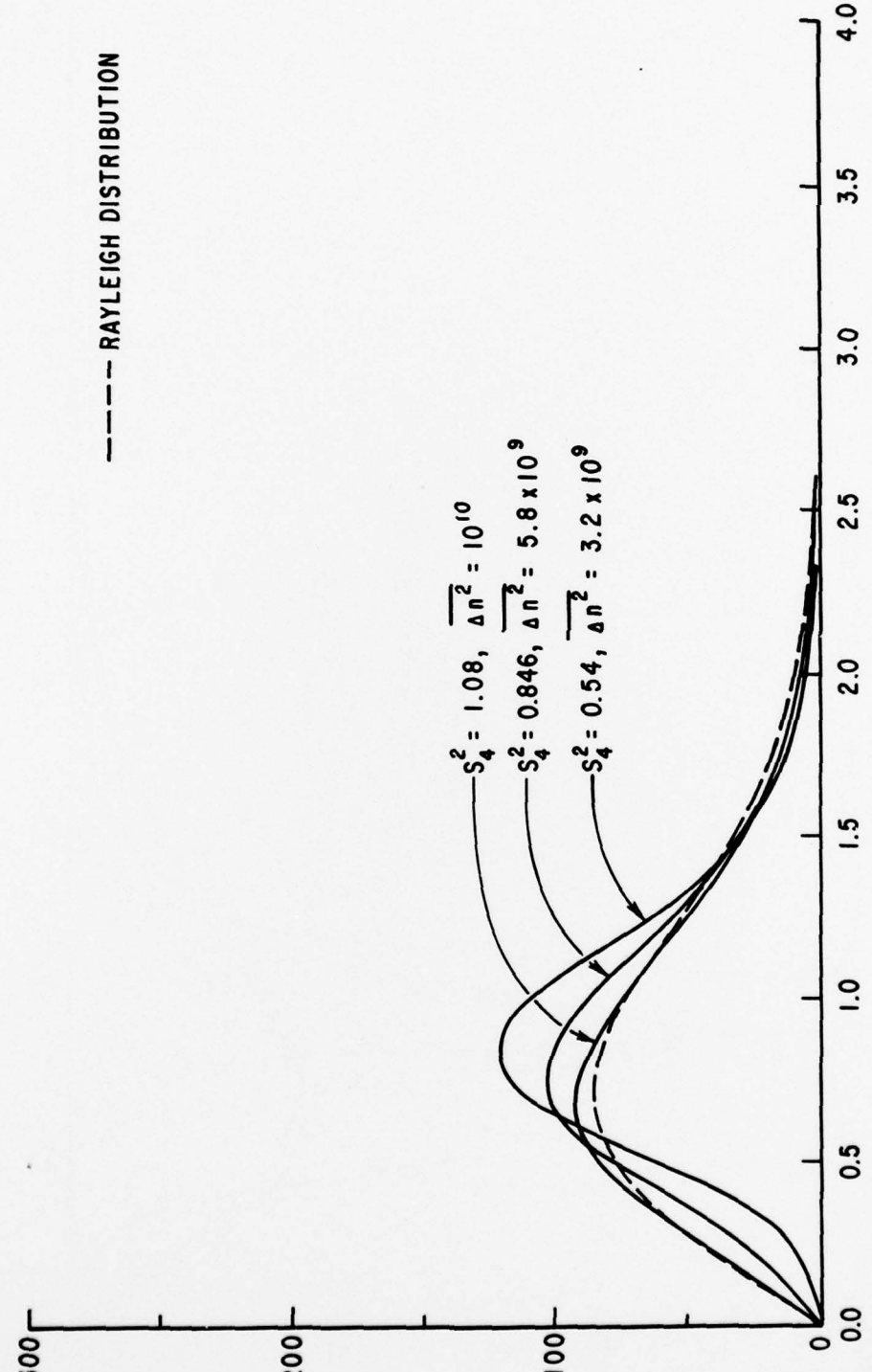

Figure 25. Amplitude Distributions for the K_ρ^{-2} Spectrum With L = 5.0 Km.

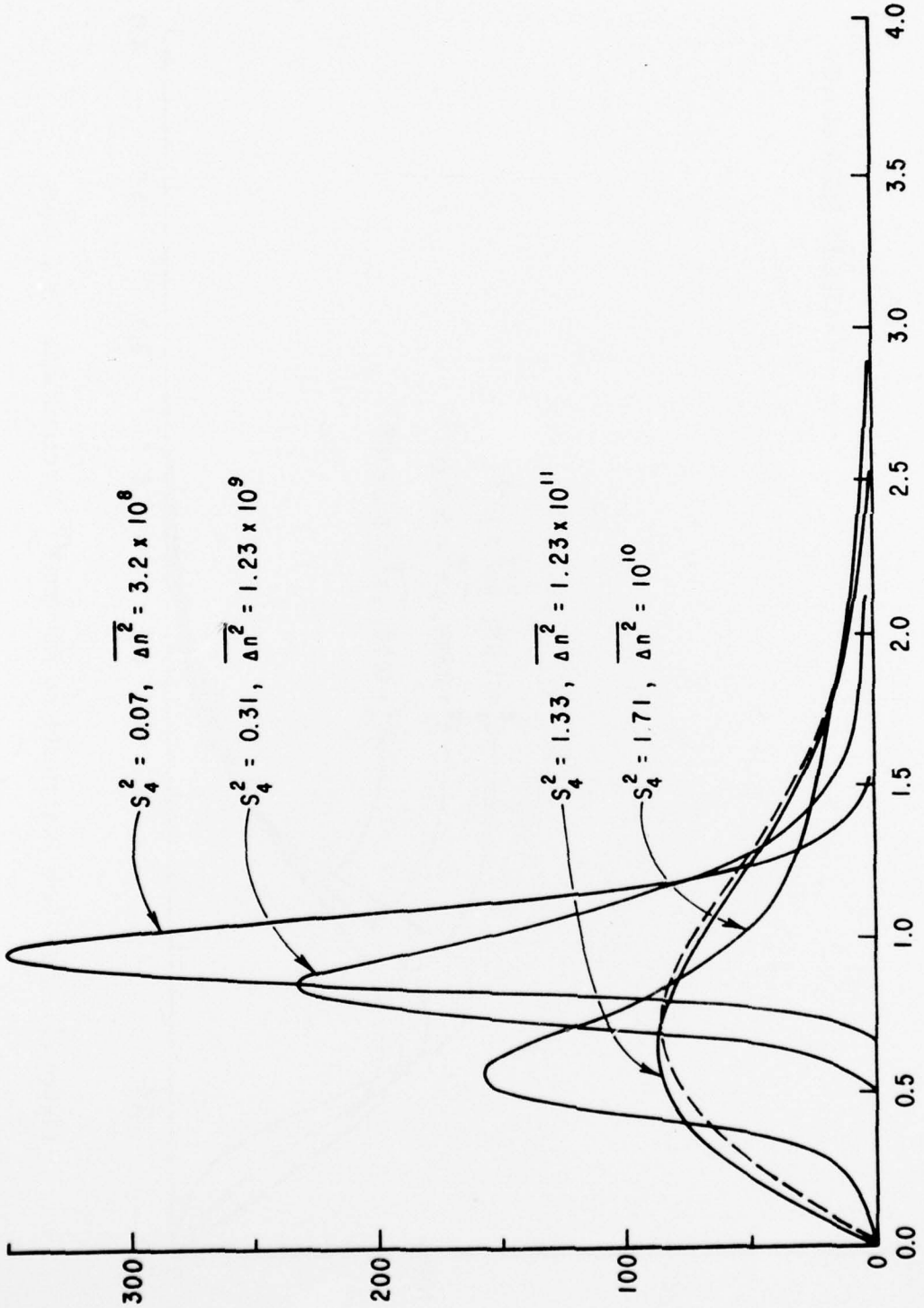

Figure 26. Amplitude Distributions for the Intermediate Spectrum.

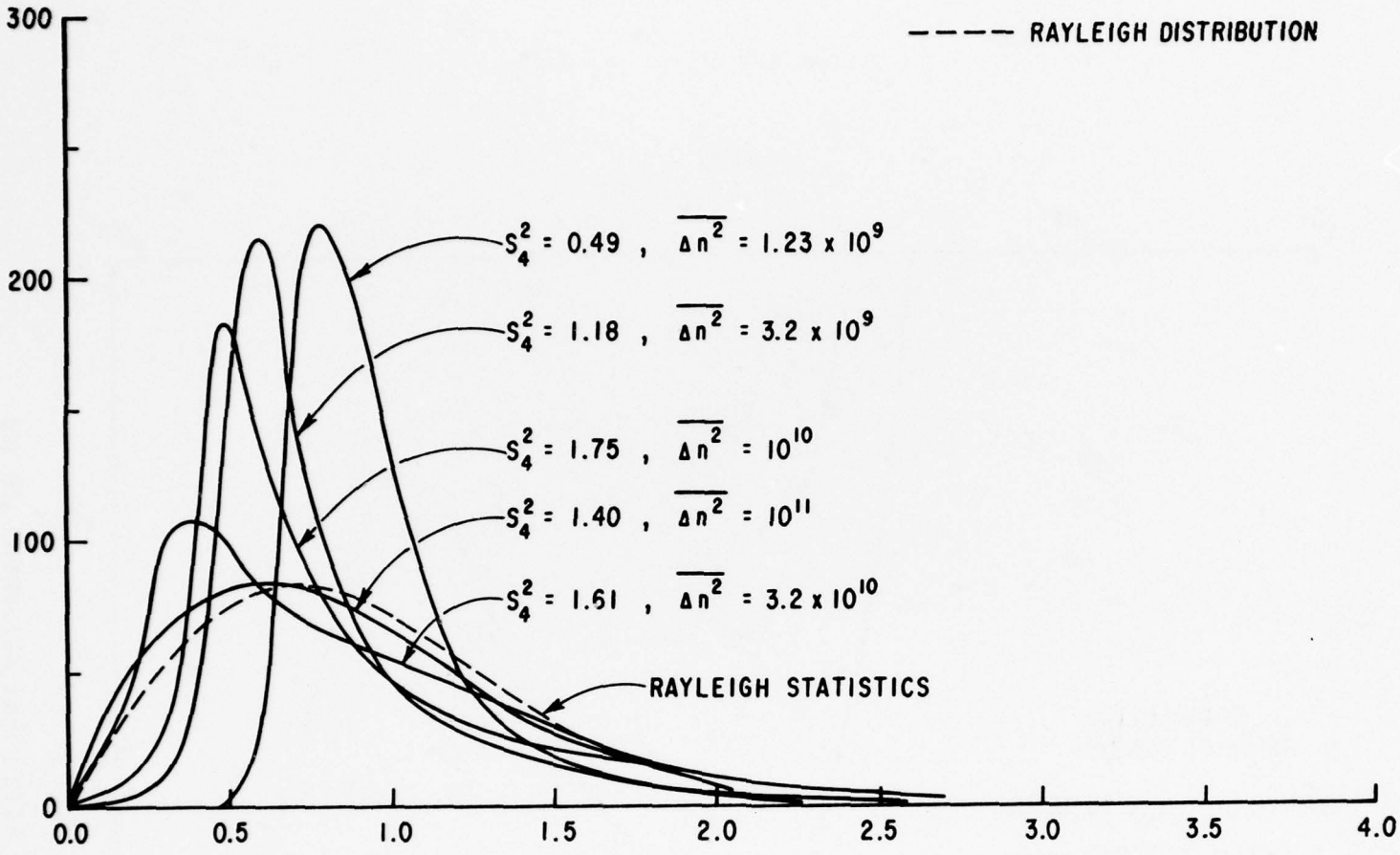

Figure 27. Amplitude Distributions for the Gaussian Spectrum.

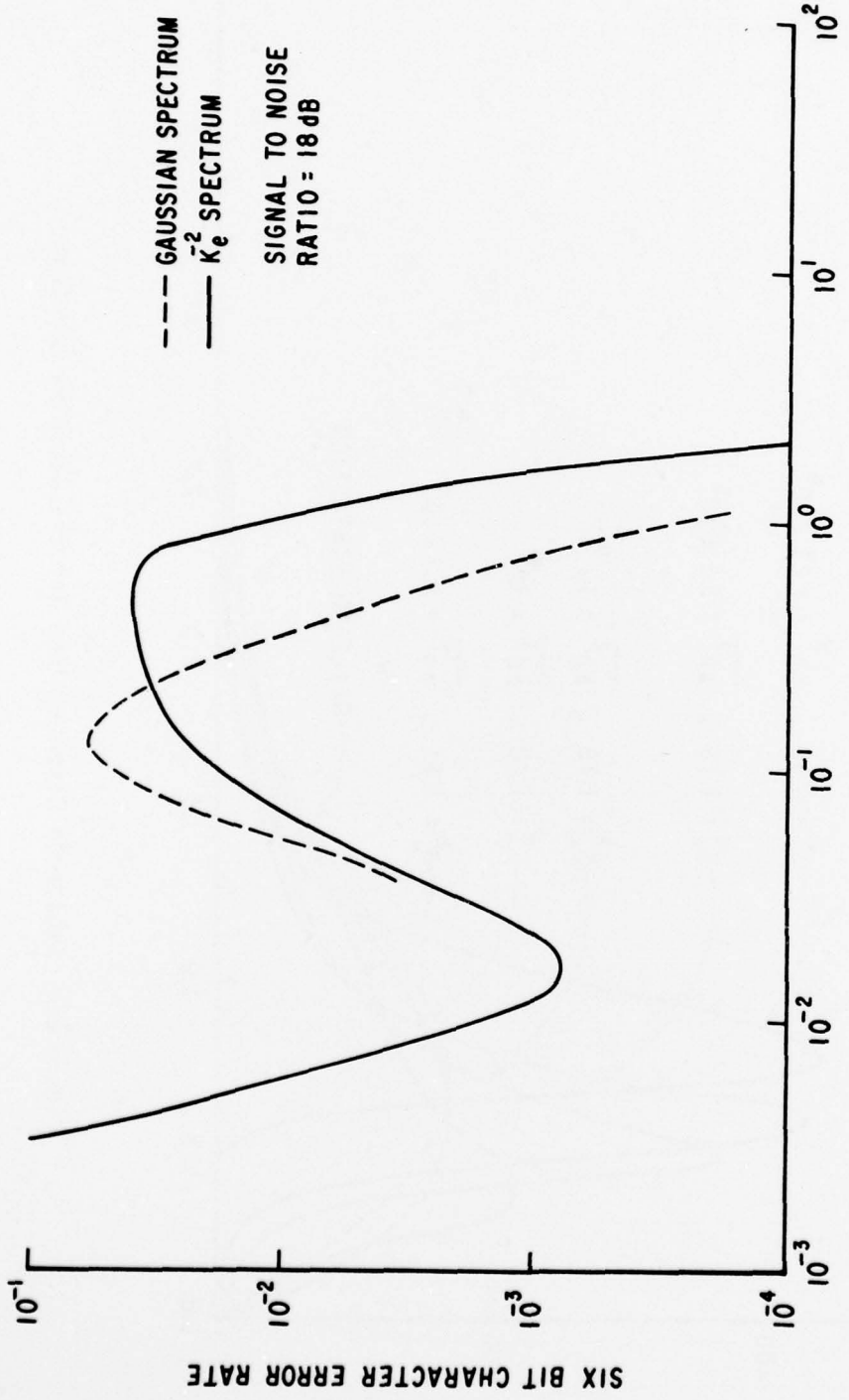

Figure 28. TATS Performance.

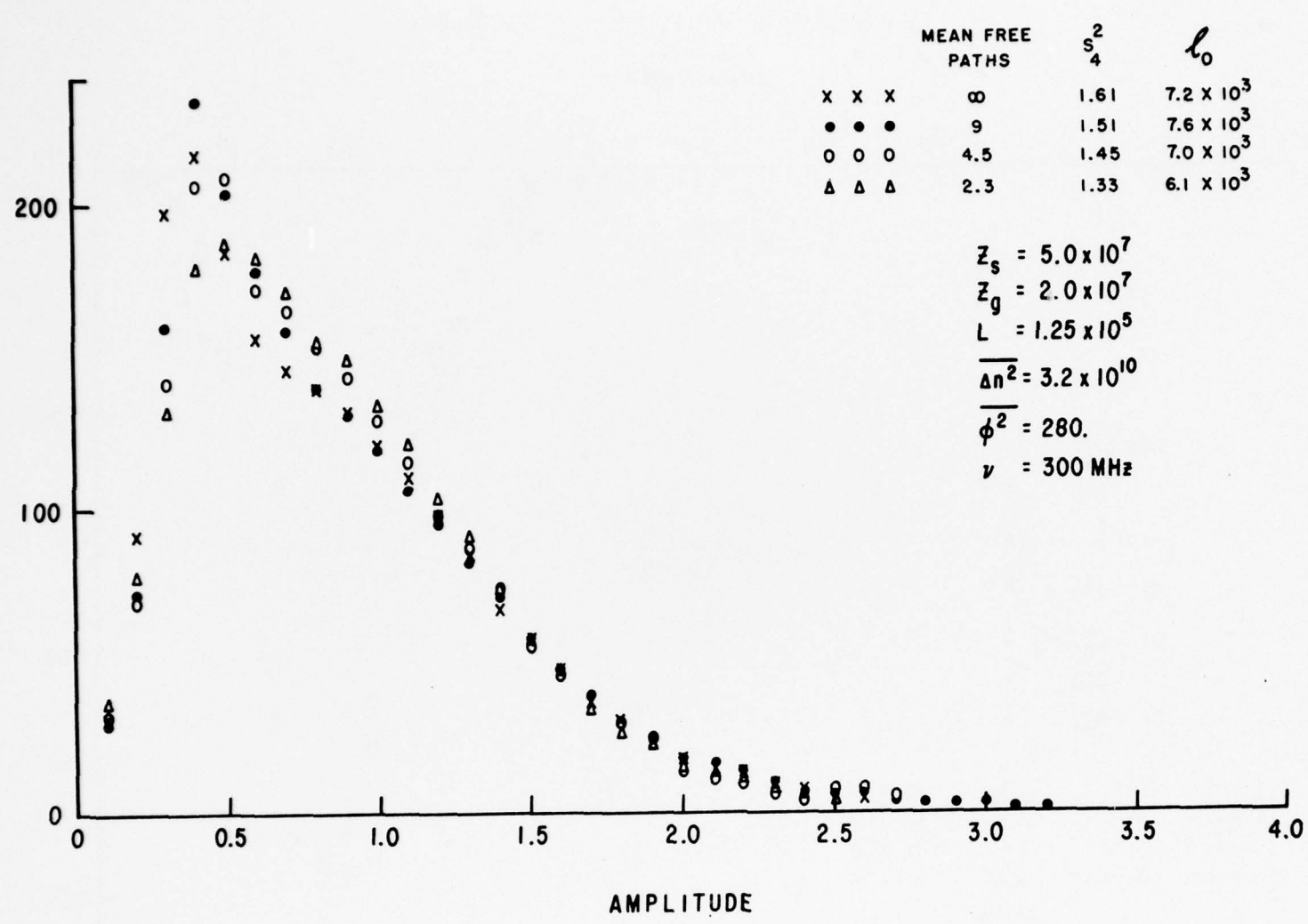

Figure 29. Gaussian Amplitude Distributions.

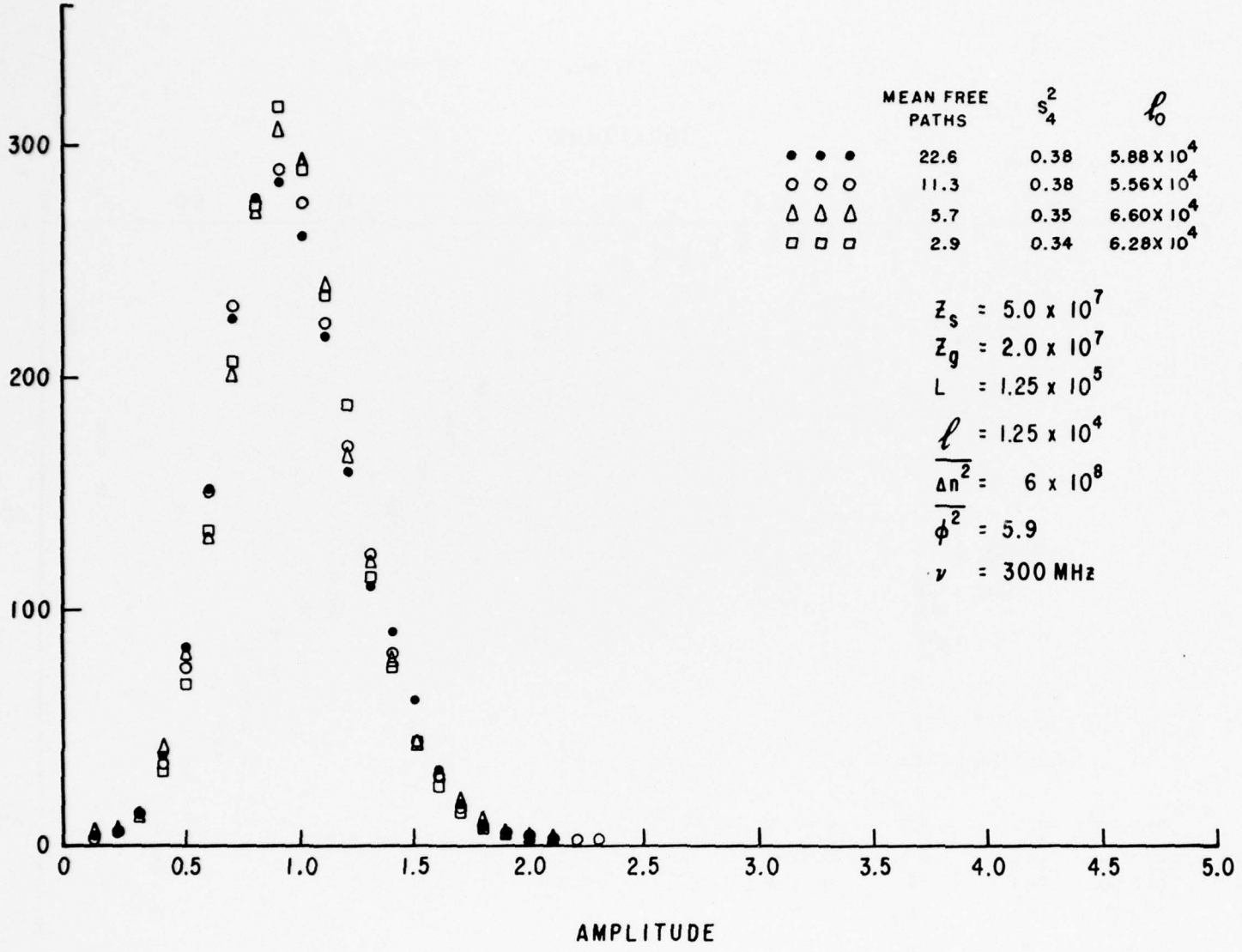

Figure 30. K_ρ^{-2} Amplitude Distributions.

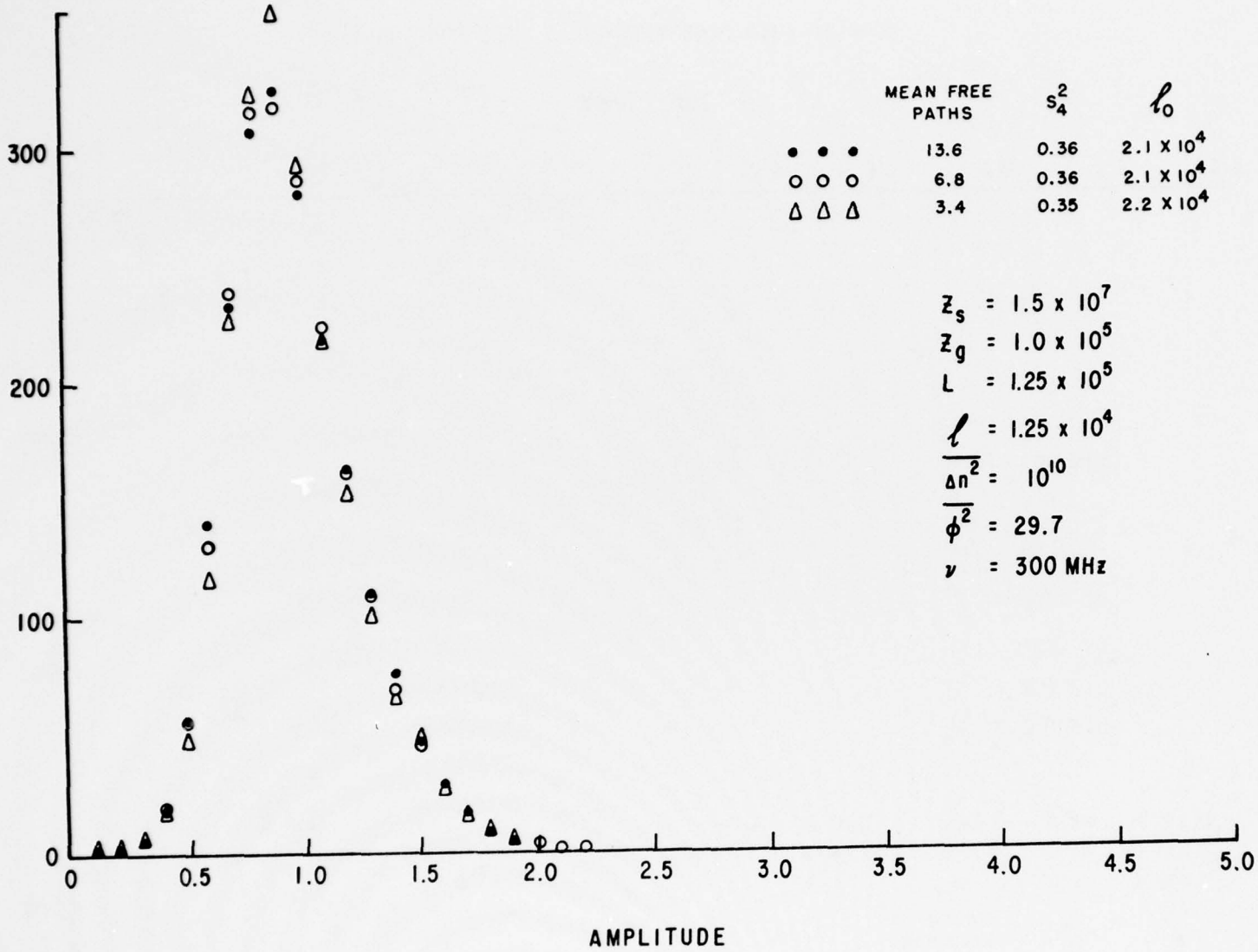

Figure 31. K_ρ^{-2} Amplitude Distributions.

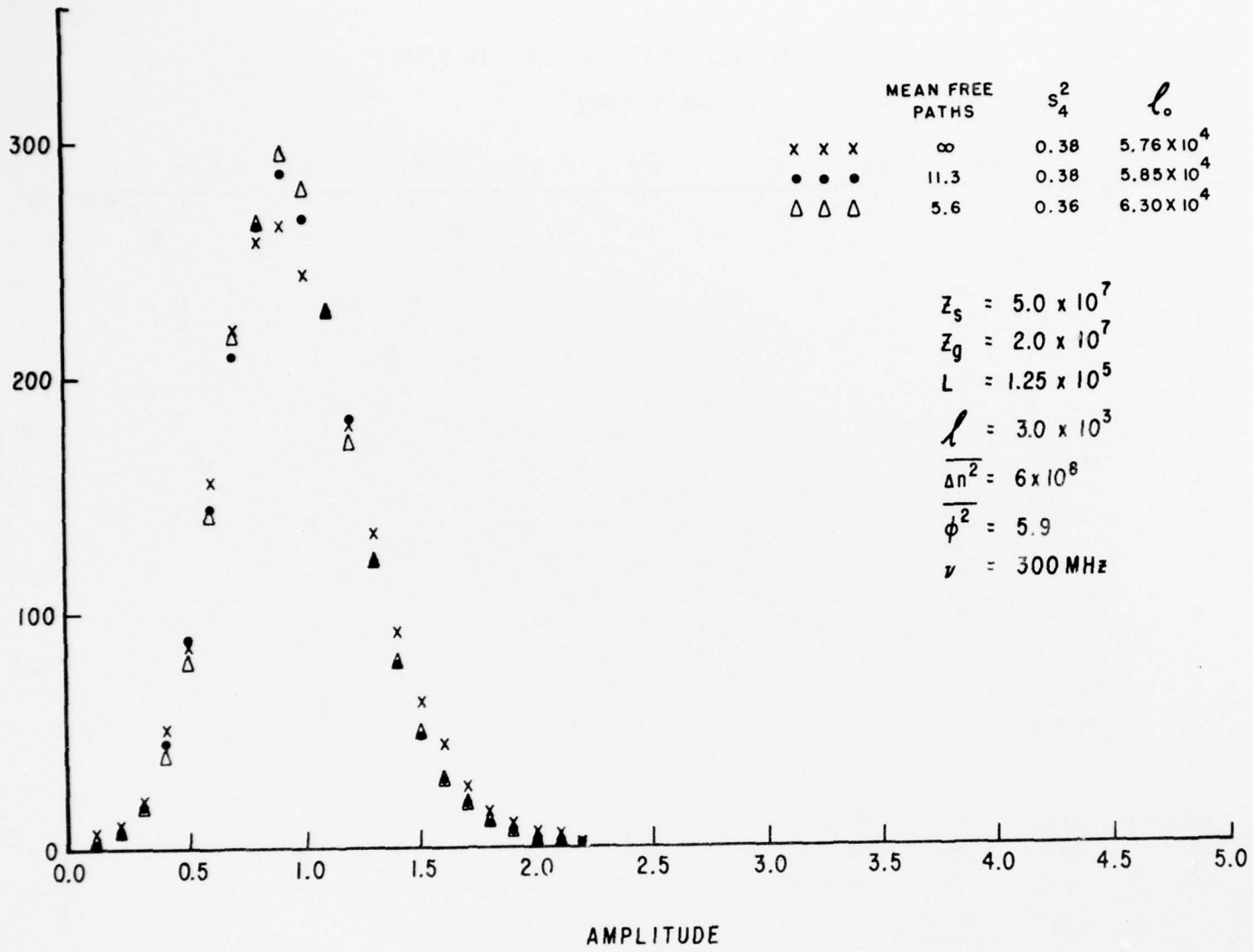

Figure 32. K_ρ^{-2} Amplitude Distributions.

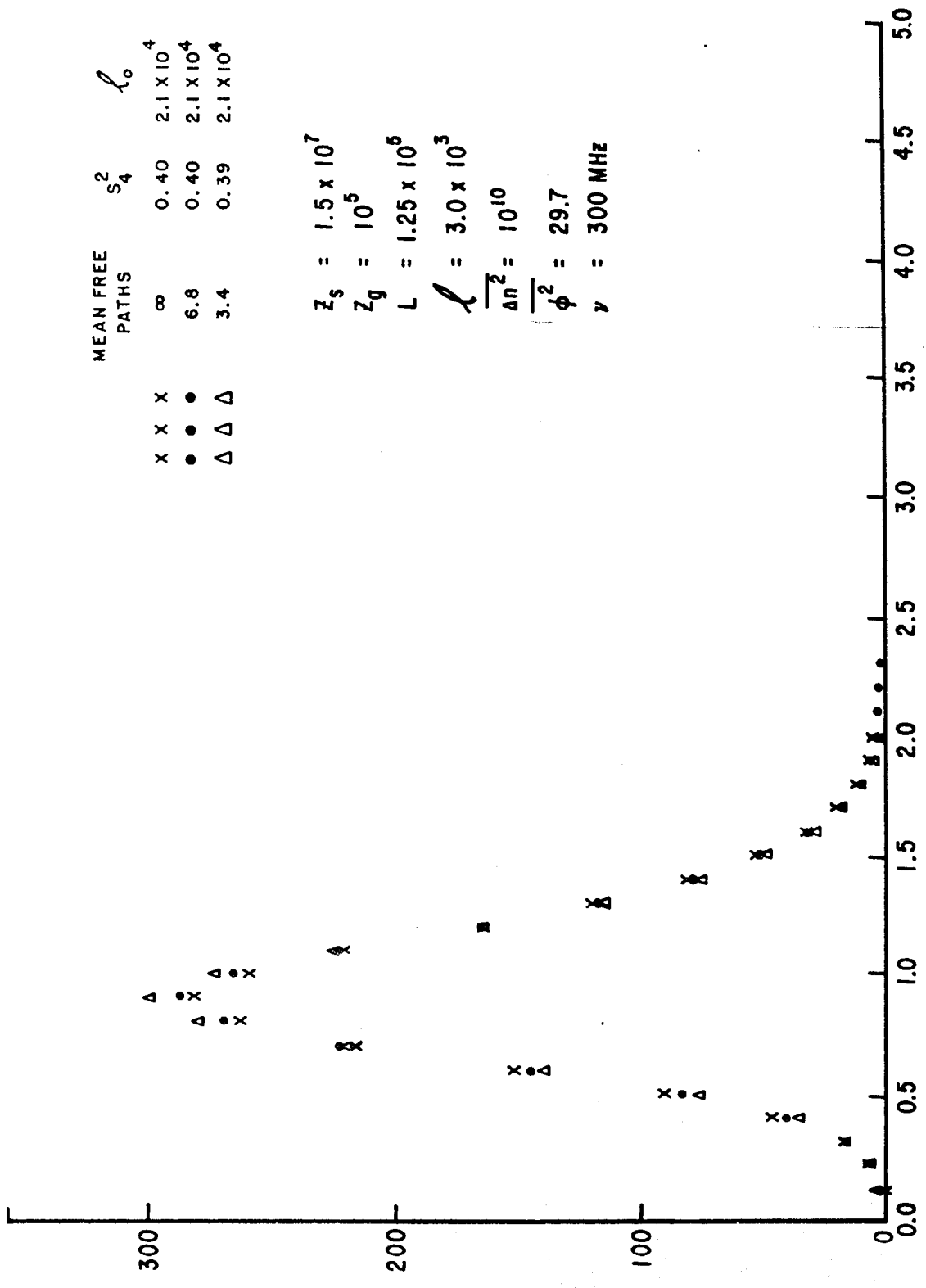

Figure 33. K_ρ^{-2} Amplitude Distributions.

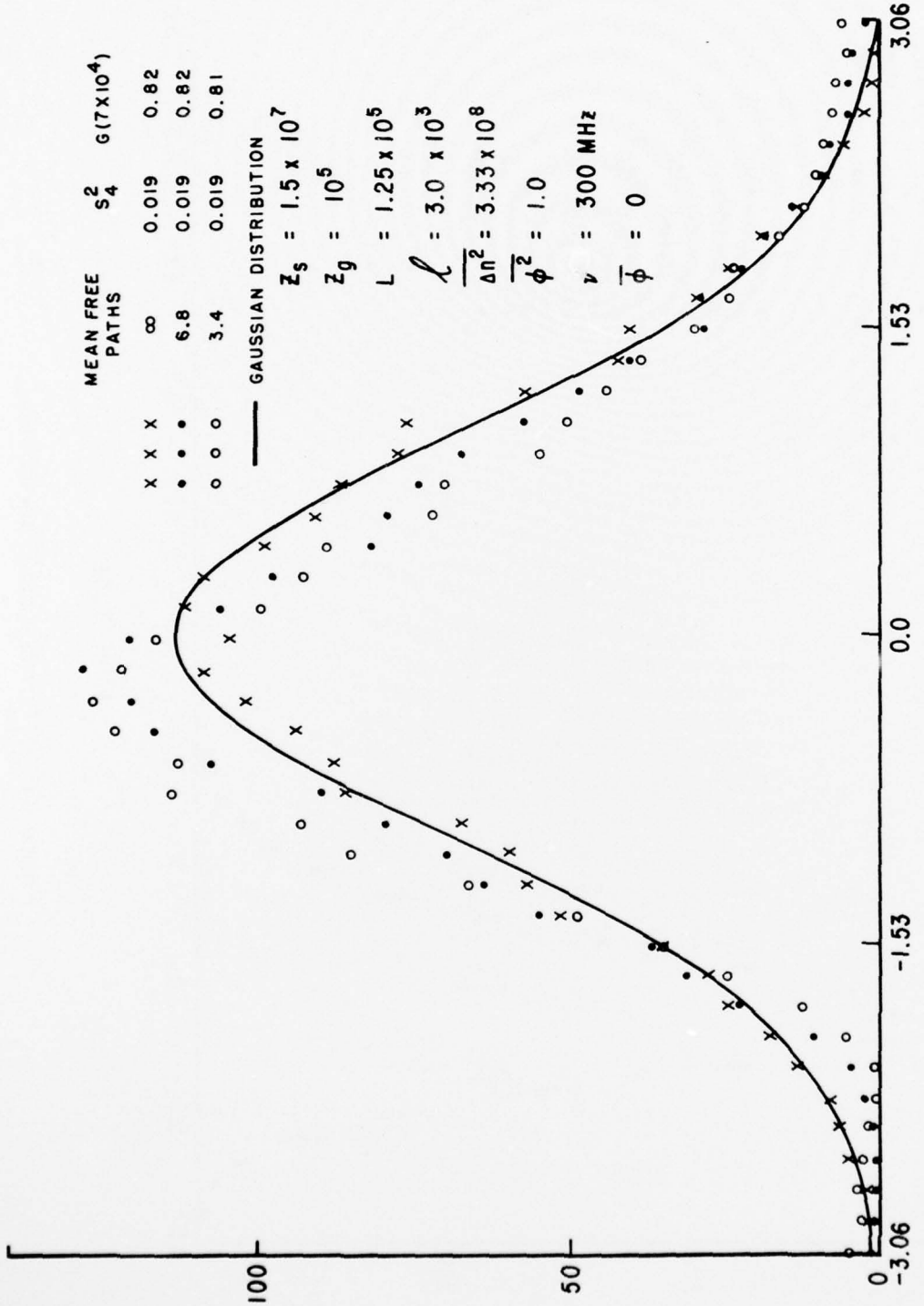

Figure 34. K_ρ^{-2} Phase Distributions.

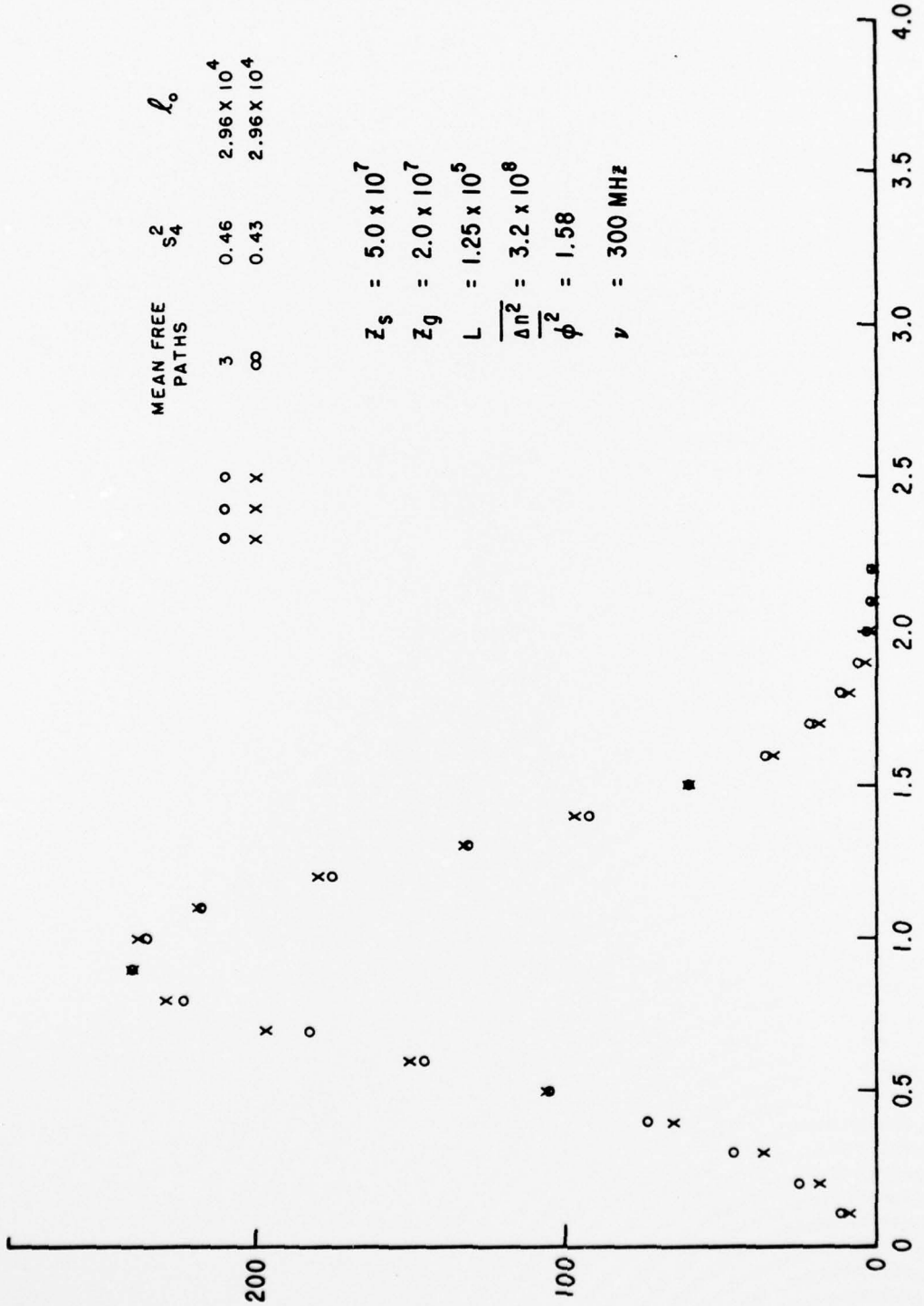

Figure 35. Square Top Hat Amplitude Distributions.

DISTRIBUTION

Hq USAF (RDQPN/1D425), Wash, DC 20330 1

AFTAC (TAP), Patrick AFB, FL 32925 1

Dir Nuc Surety (SN), Kirtland AFB, NM 87117 1

AUL (LDE), Maxwell AFB, AL 36112 1

AFIT (Tech Lib/Bldg 640), WPAFB, OH 45433 1

USAF, SCLO (Maj Pierson/Ch, LO), POB 348, Toronto, ON, Canada M5K 1K7 1

AFSC, Andrews AFB, Wash, DC 20334
(DLSP) 1
(DLCAM) 1

CINCSAC (DOXS), Offutt AFB, NE 68113 1

ADC (XPQY), Ent AFB, CO 80912 1

SAMSO (SEN), POB 92960, WWPC, Los Angeles, CA 90009 1

AFGL, Hanscom AFB, MA 01730 1

AFWL, Kirtland AFB, NM 87117
(HO/Dr. Minge) 1
(SUL) 2
(DYT) 5
(ELC) 5
(NTS) 2

AFOSR, 1400 Wilson Blvd, Arlington, VA 22209 1

Dir, DNA, Wash, DC 20305
(STSI) 1
(STTL) 3
(DDST) 1
(C. Fitz/P. Fleming) 2

DDR&E (Asst Dir/Strat Wpns), Wash, DC 20301 1

Dir, DIA, Wash, DC 20305 1

OSD, ARPA (NMR), 1400 Wilson Blvd, Arlington, VA 22209 1

FCDNA (FCPR), Kirtland AFB, NM 87115 1

LVLO (FCTCL), POB 2702, Las Vegas, NV 89104 1

WSEGp (Doc Cont), Wash, DC 20305 1

JSTPS (JLTW), Offutt AFB, NE 68113 1

LLL (TID), POB 808, Livermore, CA 94550 1

LASL (Rpt Lib), POB 1663, Los Alamos, NM 87545 1

DDC (TCA), Cameron Sta, Alexandria, VA 22314 2

SRI (C. Rino), 333 Ravenswood Ave, Menlo Pk, CA 94025 1

Aerosp Corp (R. Fox), POB 92957, Los Angeles, CA 93009 1

NELC (M. Paulson), San Diego, CA 95152 1

SAI (D. Sachs), POB 2351, La Jolla, CA 92037 1

MRC (R. Bogusch), PO Drawer 719, Santa Barbara, CA 93102 1

Phys Dyn Inc. (J. Workman), POB 1069, Berkeley, CA 94701 1

NRL (S. Ossakow), Wash, DC 20375 1

Elec Sys Lab (J. Marshall), 495 Java Dr, Sunnyvale, CA 94086 1

SAMSO/SKA (Maj Reining), POB 92960, WWPC, Los Angeles, CA 90009 1

AFGL (J. Aarons), Bedford, MA 01731 1

DISTRIBUTION

DARPA/IPTO (Cmdr F. Hollister), 1400 Wilson Blvd, Arlington, VA 22209	1
ESD/DCKD/53 (LtC J. Crocco), Hanscom AFB, MA 01731	1
MIT-Lincoln Lab (E. Bucher), POB 73, Lexington, MA 02173	1
GE-TEMPO (DASIAC), Santa Barbara, CA	1
FCDNA (FCPRL), Livermore, CA	1
Official Record Copy (Capt Wittwer, AFWL/DYT)	1